MARMARA UNIVERSITY
FACULTY OF ENGINEERING
MECHANICAL ENGINEERING

DESIGN AND OPTIMIZATION OF THERMOFORM DIE TO MINIMIZE ENERGY USE BY MEANS OF FLUID SOLID INTERACTION (FSI) ANALYSIS

Muhammet Metehan ARSLAN

Mutlu DİLGİÇ

GRADUATION PROJECT REPORT

Department of Mechanical Engineering

Supervisor

Assoc. Prof. Mustafa YILMAZ

ISTANBUL, 2024

MARMARA UNIVERSITY

FACULTY OF ENGINEERING

Design and Optimization of a Thermoform Die to Minimize Energy Use by Means of Fluid Solid Interaction (FSI) Analysis

by

Muhammet Metehan ARSLAN

Mutlu DİLGİÇ

June 11, 2024, Istanbul

SUBMITTED TO THE DEPARTMENT OF MECHANICAL ENGINEERING IN PARTIAL FULFILLMENT OF THE REQUIREMENTS FOR THE DEGREE

OF

BACHELOR SCIENCE

AT

MARMARA UNIVERSITY

Signature of Author(s) **Muhammet Metehan ARSLAN**

. **Mutlu DİLGİÇ**

Department of Mechanical Engineering

Certified By **Assoc. Prof. Mustafa YILMAZ**……..

Project Supervisor, Department of Mechanical Engineering

Accepted By **Prof. Dr. Bülent EKİCİ**…….

Head of the Department of Mechanical Engineering

TABLE OF CONTENTS

ACKNOWLEDGEMENTS

First of all, we would like to thank our supervisor Assoc. Prof. Mustafa YILMAZ for the valuable guidance and advice on preparing this thesis and giving us moral and material support. We were able to complete our thesis with his help and direction. Thanks to his guidance and instruction, we are now better engineers, capable of solving complicated technical issues via analysis and with sharper critical thinking abilities.

We would like to express our gratitude to our dear friend Miraç Oymak, who has years of experience in the thermoform molding industry for showing us her continuous support and cooperation.

ÖZET

Termoform kalıpçılık sektörü dünyada ve ülkemizde plastiğin kullanımının birçok alanda artmasıyla oldukça yaygınlaşmıştır. Günümüzde birçok alanda kullanılan termo plastiklerin işlenme kolaylığı ve ucuzluğundan ötürü özellikle plastik ambalajlar fazlasıyla insan hayatının içindedir.

Bizim bu çalışmayı yapmaktaki amacımız termoform kalıpçılık sektöründe kase-kapak ambalajının üretim sürecindeki hava ile ürünün kalıptan ayrıldığı işlem üzerinde birim zamanda harcanan enerjiyi, zamanı, iş gücünü optimize etmek ve elde edilen ürünün kalitesine artırmaktı. Bunun için 3 boyutlu tasarım ve hesaplamalı akışkanlar mekaniği analizi yapabilen bir bilgisayar programında kendi tasarımlarımız ve analizlerimizi yaparak oldukça dikkate değer, bu sektör için göze çarpar derecede verimli sonuçlar elde ettik.

Özellikle ülkemiz açısından bu sektördeki bizim yaptığımız bu tip geliştirmelerin eksikliğinin farkındayız. Yaptığımız çalışmadan aldığımız sonuçlar bunu açık bir şekilde kanıtlıyor. Umarız ki bu ve daha birçok çalışma reel endüstriyel alanda dikkate alınır ve insanların hayatı çok daha kolaylaşır

ABSTRACT

The thermoform molding industry has become widespread in the world and in our country, with the increased use of plastics in many areas. Due to the ease of processing and cheapness of thermoplastics used in many fields today, especially plastic packaging is a major part of human life.

In the thermoform molding industry, our aim was to optimize the energy, time, and workforce spent in the process of producing the air and the unit-time process in which the product is separated from the mold, and to improve the quality of the resulting product. We have achieved remarkable results for this industry by doing our own designs and analyses in a computer program that can do 3D design and calculated fluid mechanics analysis.

Especially for our country, we are aware of the lack of such improvements that we have made in this sector. The results we have obtained from the work we have done clearly prove this. We hope that this and many more studies will be taken into account in the real industrial field and that people's lives will be much easier.

SYMBOLS

Symbol	Name	Unit
T_g	Glass transition	℃
T_m	Melting temperature	℃
C_{fc}	Coulomb's Friction Coefficient	
P_{atm}	Atmospheric pressure	$\frac{N}{m^2}$
ρ	Density	$\frac{kg}{m^3}$
C_p	Heat capacity	$\frac{J}{kg.℃}$
k	Thermal conductivity	$\frac{W}{m.K}$
q_{abs}	Heat absorbed	J
t	Time	s
z	Thickness	mm

ABBREVIATIONS

PET	Polyethylene Terephthalate
PS	Polystyrene
HIPS	High Impact Polystyrene
PVC	Polyvinyl Chloride
ABS	Acrylonitrile Butadiene Styrene
PMMA	Poly(methyl methacrylate)
DMA	Dynamic Mechanical Analysis
FW	Forming Window
T	Thermal
M	Mechanical
FSI	Fluid Solid Interaction
TM	Thermomechanical
VA	Vaccuum Assisted Thermoforming
PA	Plug Assisted Thermoforming
H	Hyperelastic Model
VE	Viscoelastic Model
VEP	Visco-elasto-plastic Model
LF	Lower Forming
UF	Upper Forming

LIST OF FIGURES

LIST OF TABLES

1. INTRODUCTION

"Thermoforming" is a category of thermoplastic sheet-forming techniques during which a thermoplastic sheet is firstly softened by heat above its glass transition temperature, then subsequently deformed by bringing it into contact with the walls of a mold, and finally cooled to obtain a shell-like product [1]. Thermoformable thermoplastics are semi-products obtained by transforming pellets into flat sheets using standard forming processes such as extrusion and calendaring [2]. Thermoforming procedures can be classified as thin gauge (thickness ≤0.25 mm), medium-weight (thickness ∈ [0.25;1.5] mm), or heavy-sheet gauge (thickness > 1.5 mm) [1].

1.1 Applications and production market

Much of the inceptions of thermoforming processes emerged just before World War II when acrylic sheets were thermoformed to produce airplane canopies [3]. Since that period of time, versatile thermoplastics have found their place in a wide range of daily-life applications and high-technologicalvalue products. In the year 2020, the global thermoforming market was estimated at 12.38 billion US dollars, with a projected annual growth of almost 4% between 2021 and 2028, as shown in Figure 1 [4].

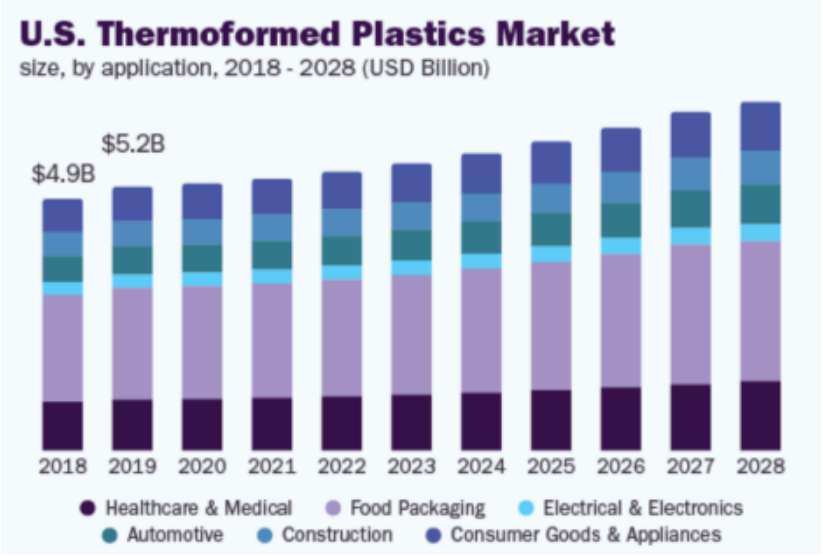

Figure 1: Thermoforming market estimates [4]

Amorphous thermoplastics such as polystyrene (PS), high impact polystyrene (HIPS), PVC, ABS, and PMMA are commonly utilized in contemporary applications. Most of these applications revolve around merging. The complex multilayer products utilize the physicochemical properties of different thermoplastics. Table 1 presents a summary of important uses for thermoformable amorphous thermoplastics, derived from a concise evaluation of patents and scholarly literature.

Table 1: Applications of standard thermoformable amorphous thermoplastics

Thermoformable amorphous thermoplastics		**HIPS**	**PS**	**PMMA**	**PVC**	**ABS**	**PC**
T_g (°C)		96	90	100	90	90-120	150
Forming window (°C)		160-205	150-190	150-190	110-150	150-205	175-230
Daily life products	**Food packaging** [2,5–7*] Disposable containers, Serving trays, Plastic cups	[8]*	[9]*	[10]*			
	Healthcare and medical [2,11*] Cosmetic cases, Trays, Tablet packaging	[8]*			[12]*		
	Consumer goods [13] Masks, Textured surfaces Inner liner of refrigerators	[8]*	[9]*	[10]*			
High technology products	**Electronic components** [14–17] 2.5 D shaped circuits, Encapsulation of printed circuit board assemblies	[8]*					
	Transport sectors [2,3] Car dashboards, Compartment doors, Aircraft cabin wall panels,	[8]*			[2]	[2]	[18]*

Amorphous thermoplastics are gaining popularity due to their broad forming window (FW) and rubber-like properties. Thermo-mechanical phenomena occurs above the glass transition (Tg) and extends across a few dozen.of degrees [2, 19]. A material's thermoformability depends on its ability to endure substantial deformations while maintaining stiffness to prevent the pre-heated sheet from flowing. FW may be determined using temperature sweeps using Dynamic Mechanical Analyses (DMA)

[20,21] and observing the evolution of storage moduli, as shown in Figure 2. Most amorphous thermoplastics have FW values ranging from 30–60 °C above Tg [20]. Semi-crystalline thermoplastics often undergo a transition from a rigid to a flexible state when they reach their melting temperature (Tm). The present report specifically examines the process of thermoforming amorphous thermoplastics.

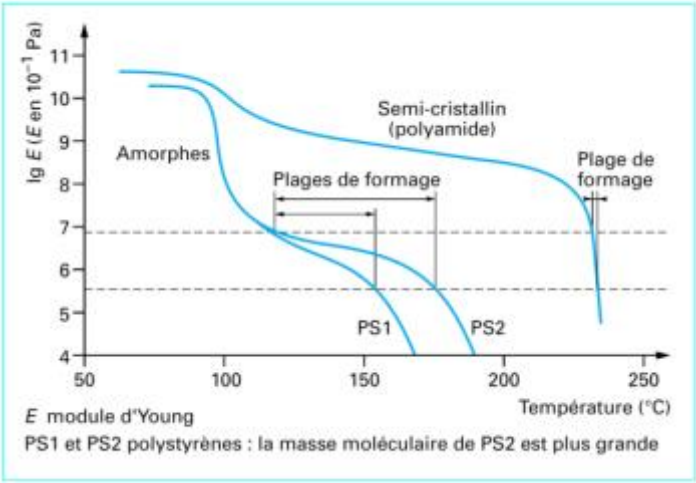

Figure 2: Theoretical variation of Young modulus according to temperature for amorphous and semicrystalline polymers [20]

1.1.1 Thermoforming cycle: Correspondence between technological operations and underlying physics

Thermoforming includes substantial deformations, both within and outside the plane, of flat thermoplastic sheets to create 3D hollow shapes. The thermoforming cycle employs a progressive procedure to attain the desired shape without excessively stretching the sheet. Figure 3 illustrates the sequence of actions, sometimes referred to as operations. This research specifically examines plug-assisted thermoforming approaches.

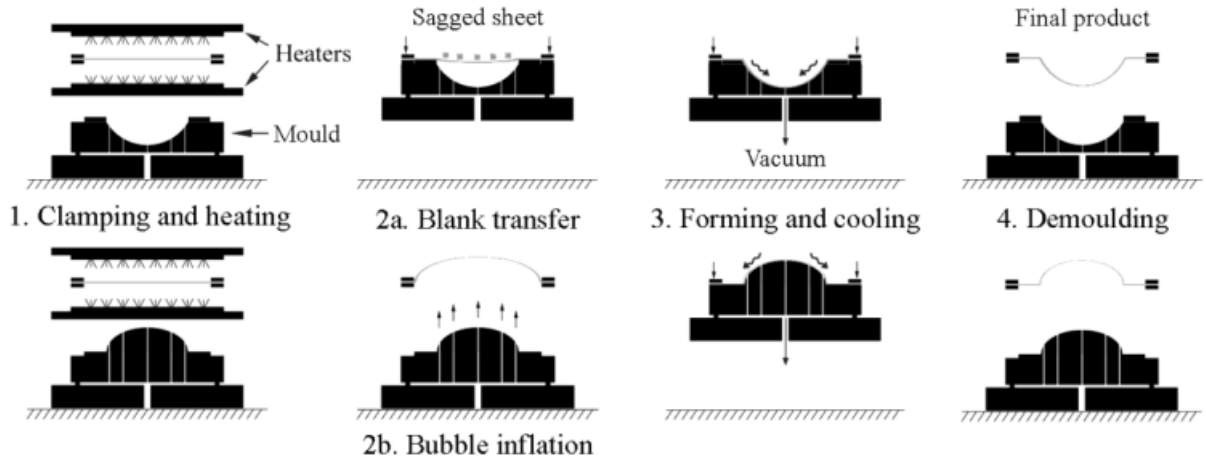

Figure 3: Steps of negative (top) and plug assisted (bottom) thermoforming processes [22]

The initial phase involves securing the borders of the sheet (Figure 4). Clamping is a mechanical constraint that restricts all possible movements (such as displacements and rotations) of the thermoplastic sheet to its edges. Let's examine a specific point M located on the surface of a thermoplastic sheet $\Omega sheet$. This point is surrounded by the peripheral Γ_sheet, as shown in Figure 4. Clamping refers to the process of applying initial mechanical boundary conditions, denoted as $BC0$, and can be described as follows:

$$\forall M \in \Gamma\_sheet \rightarrow \{x_M = y_M = z_M = 0; \qquad (1)$$

Where, xM, yM, zM are displacements and rxM, ryM, rzM are rotations at the material point M within a Cartesian coordinates system associated with the sheet.

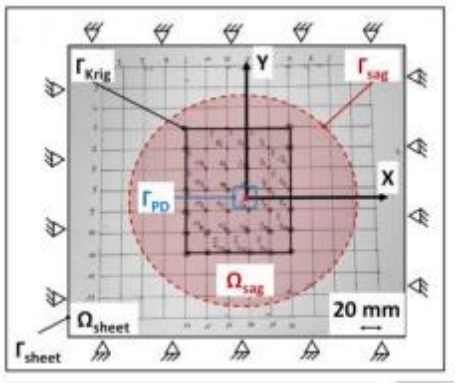

After applying the initial mechanical boundary conditions ($BC0$) to the flat sheet, the heating stage begins (Figure 3.1).

Figure 4: Considered domains of interest (Ω) and applied initial boundary conditions on the edges of the sheet (Γsheet) [23]

Technologically, thermoforming machines are fitted with radiation heating ovens made of ceramic components or halogen lamps that emit infrared light. Heating can be achieved by exposing one or both sides of the thermoplastic sheet to radiation heating ovens, depending on the equipment utilized and the thickness of the sheet. The technique involves raising the temperature by creating temperature gradients through the thermoplastic material [24,25]. The heating step concludes when the material's temperature reaches the FW [26]. Thermal deformations result in the loss of the original boundary conditions (BC0) of the thermoplastic sheet.

After the heating stage, the next process involves pre-stretching or inflating the material using air pressure in the forming chamber. This results in a favorable pressure difference between the softened sheet and the plug, enabling deformation during air blowing activities (Figure 3.2).

$$M \in \Omega_{sag}; \{|P - P_{atm}| > 0;\ T(t) \geq T_g\} \qquad (2)$$

In this equation, $Patm$ represents the atmospheric pressure and P represents the pressure applied. After prestretching, the sheet is shaped or molded. A solid-to-solid contact mechanical load is used to aid in substantial out-of-plane deformation of the sheet using a plug. During the plug-assisted thermoforming process (negative or positive), the mold typically has a lower temperature than the sheet [5, 27]. To achieve substantial deformations without breaking the product's walls, the forming time is kept short (at most a few seconds) [28].

After the manufacturing process, the sheet is cooled using non-thermally conditioned air (Figure 3.3). By reducing the temperature of the sheet below its glass transition temperature (Tg), the material's rigidity rises while maintaining the sheet's deformed shape. The product that has been manufactured is removed from the mold, released from any clamps, and then cut to the desired shape (see to Figure 3.4).

1.2 Industrial Context: Common thermoforming-induced flaws

Industrial R&D for thermoforming thermoplastics focuses on balancing cost and product quality. Indeed, lowering costs and eliminating waste necessitates (i) shortening cycle times and (ii) optimizing each elementary operation by overcoming the relevant process-

induced faults (see Section 1.1.2). Technological challenges include limited control over temperature distributions [29, 30], high thickness variation in thermoformed products [31-33], high risk of sheet rupture in complex geometries [1, 34], and irregularities in local material properties due to processing history [35-38]. Several studies have proposed technological solutions to overcome the challenges, including differential heating [1], air pressure to prestretch the softened sheet after heating [32, 39], and plugs for large out-of-plane deformations [40]. Nonetheless, existing technology solutions may complicate the procedure.

1.2.1 Temperature heterogeneity following the heating stage

As stated in Section 1.1.2, infrared heating ovens are used to heat the core of thermoplastic sheets. Heating quality and temperature field homogeneity are influenced by (i) the material point's proximity to the infrared emitting element, (ii) its depth within the sheet, and (iii) the heating element's efficiency in relation to the polymer's emissivity [29]. The dominant heat-transfer methods are classified into two geographic domains based on thermal energy balance. Figure 5a shows the first spatial domain, which includes the infrared emitting components and the sheet's exposed surface. Heat transmission in this domain occurs by convection and radiation [30]. Heat is transported throughout the material in the second spatial domain through the processes of radiation absorption and thermal conduction between the surface and core. For single-sided infrared heating (as seen in Figure 5b), the heat distribution across the thickness can be described by a transient heat equation.

$$\rho C_p \frac{dT}{dt} = k \frac{d^2T}{dz^2} + \dot{q_{abs}} \qquad (3)$$

Where, ρ: density [kg / m3] Cp: heat capacity [J / (kg.°C)] k: thermal conductivity [W / (m.K)]

And, z: coordinate in the thickness direction t: elapsed time since the heating start [s] $qabs$: heat absorbed from radiative heating.

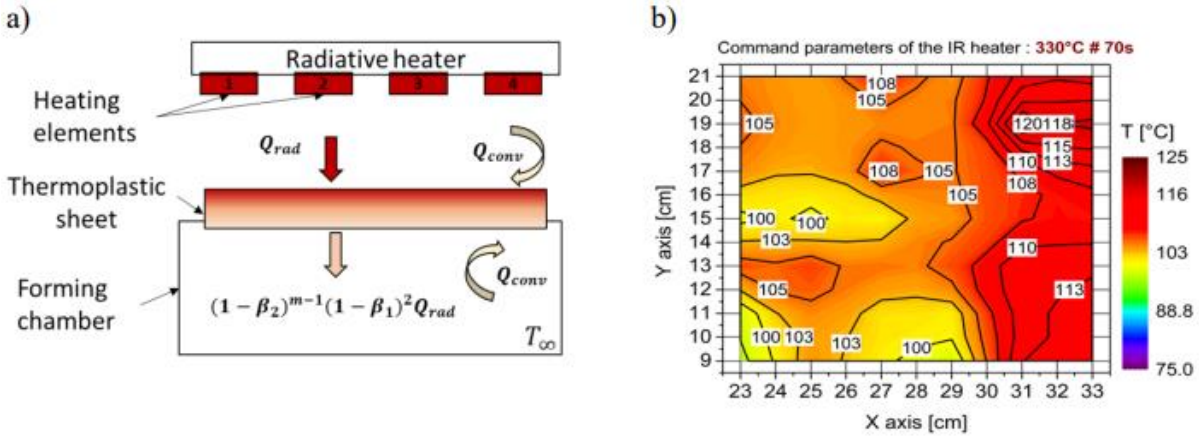

Figure 5: (a) Schema of single-side infrared heating of a thermoplastic sheet (inspired by [41]); (b) Temperature heterogeneity on HIPS sheet following single sided IR heating of a thermoforming machine [42]

From a numerical point of view, numerous studies have addressed infra-red pre-heating of polymers via: (i) modelling the transient heat transfer in the case of transparent and grey thermoplastic sheets, (ii) optimizing the calibration of infra-red heating ovens based on metaheuristics [43,44], (iii) by relying on an iterative learning model to control to the heating phase [45], or (iv) numerical simulation of the polymer heating based on the ray-tracing method [46,47].

1.2.2 Effect of temperature on initial boundary conditions

In the case of large-drape forming (large extent of the sheet), the increase of the temperature of the clamped sheet can be associated with thermal deformations induced by the relaxation of residual stresses (related to the thermo-mechanical history). The sheet is mechanically constrained on all of its sides, and it droops (or sags) due to gravity force [48]. Sagging (as shown in Figure 6) results in a change of the distance between the sheet and the infra-red heaters, and thus, it alters the efficiency of radiative heat transfer [33]. Temperature homogeneity might not always be guaranteed due to the radiative heating technique used and the resulting sagging of the sheet. The radiative energy that is absorbed into a surface from a radiative source is dependent on the solid angle that the absorbing surface subtends with the source, which influences the radiation view factor [49]. As the sagging of the sheet deforms the absorbing surface, the angle subtended by a material point on the sheet varies based upon the location. Therefore, such unbalanced

heating from the ceramic radiators of the heater causes a difference in stretching between hot zones on the sheet (T > Tg) and the comparatively cooler ones

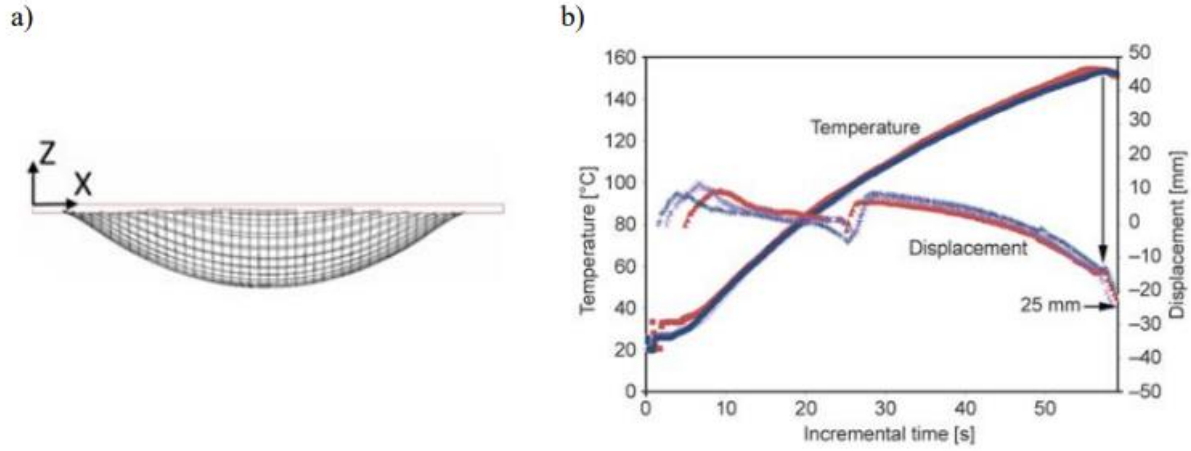

Figure 6: (a) Recording showing the sagging of the sheet followed by heating [23]; (b) Vertical displacement and temperature of the sheet as a function of time during heating stage [48]

1.2.3 Contact and friction

The final thickness of the final product is governed by the temperature difference between the thermoplastic sheet and the plug, which determines whether the mechanical behavior during the forming stage stays in the FW or it shifts to the glassy domain [5]. The friction coefficient, which characterizes the contact surface between the sheet and the plug, can also influence the final thickness [20,27,48,50]. This has been highlighted in detail in Chapter 6. Figure 7 shows the variation of friction coefficient between a HIPS sheet and an aluminum plug as obtained by Marathe et al. [27]. It can be observed from Figure 7 that the friction seems to increase from almost 0.25 below the Tg to values higher than 0.4 within the FW of HIPS

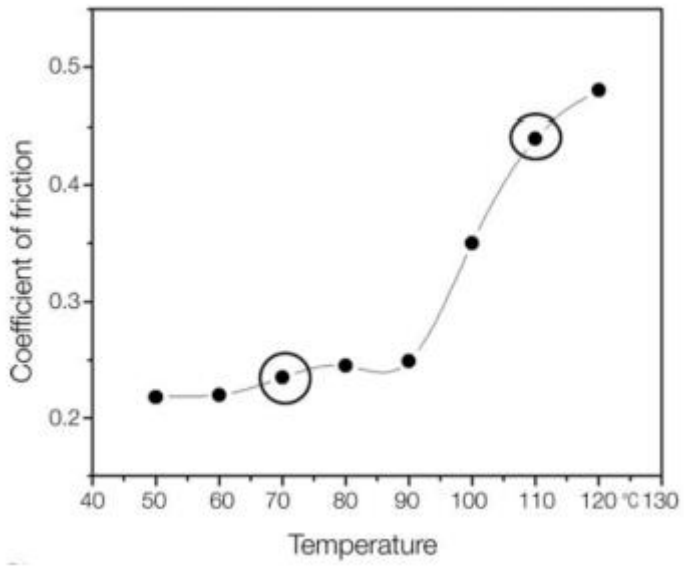

Figure 7: Coefficient of friction between a HIPS sheet and an Aluminium plug as a function of plug temperature [27]

1.2.4 Non-uniform wall thickness

One of the most significant constraints of the thermoforming process is the non-uniform thickness distribution of the resulting pieces [51]. Indeed, thin thermoplastic sheets can be considered incompressible materials. Based on volume conservation inside the material, extending the sheet along any of its principal axes would reduce its thickness. However, a thermoplastic's capacity to stretch is determined by its local behavior, which is influenced by the local temperature following IR heating. As a result, the output of a stretching operation during a thermoforming cycle is strongly dependent on the sheet being heated uniformly. Vacuum-assisted thermoforming, for example, is well known to produce components with significant thickness fluctuations throughout. The walls of the sheet are the thinnest in zones of severe drawing (shown in Figure 8), which are located in the corners of the mold and near the bottom edges [34,52]. Figure 9 shows the variation of thickness profiles at different locations from the base center of a thermoformed HIPS yogurt cup under the effect of the forming temperature. At a distance of 120 mm from the center of the plug, the sheet is at its thinnest with a variation of 11.5 % and 59.2%, respectively, for 130 °C and 140 °C compared to the measured values for 120 °C.

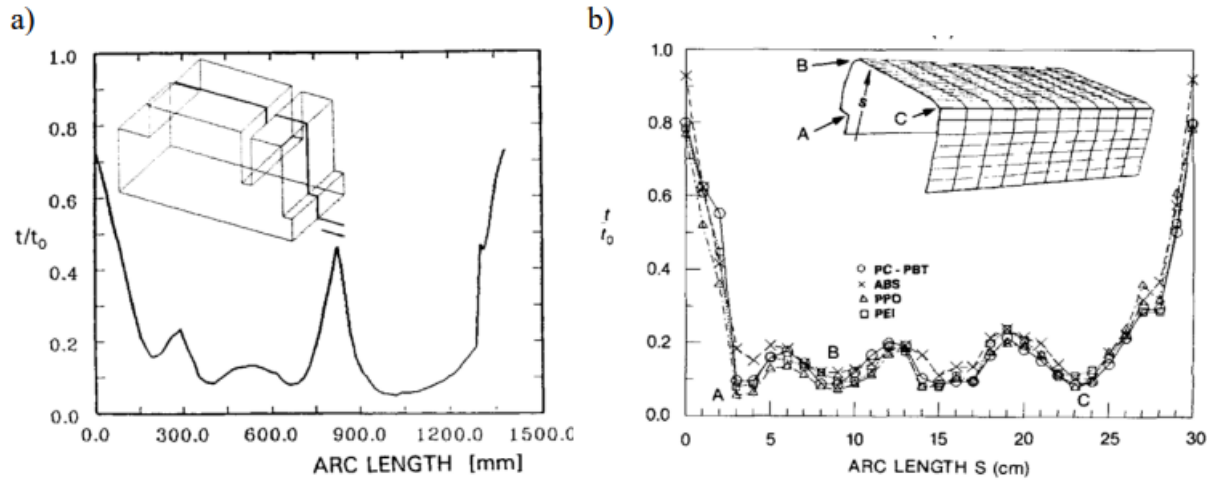

Figure 8: : Variation of thickness ratio along the length of a part with complex geometry using (a) PMMA [34] and (b) PC, ABS, PPO, PEI [52]

Consequently, mechanical stretching can result in uneven thickness distribution, which might drop below the critical minimum for which the product has been designed [5,53].

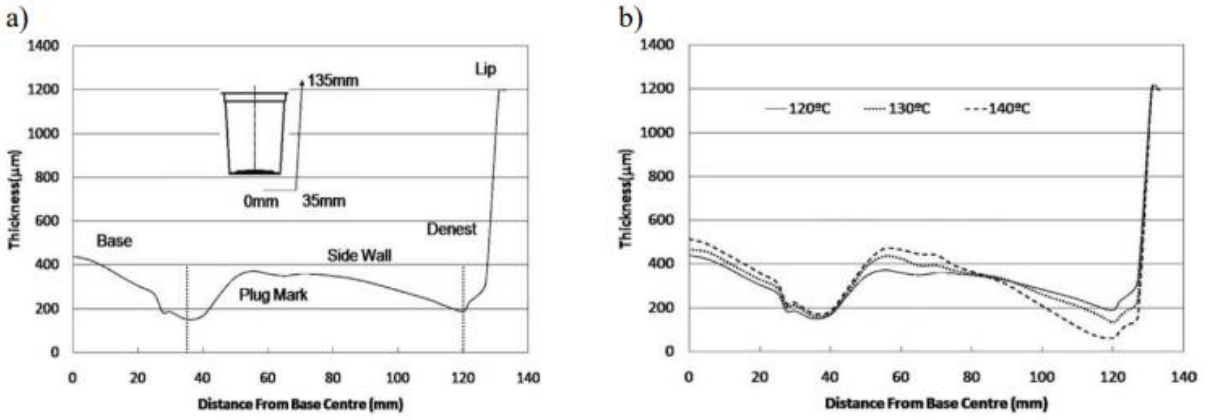

Figure 9: (a) Thickness profile of a plug assisted thermoforming part from HIPS sheet at 120°C temperature; (b) Variation of thickness profile for different sheet temperatures [5]

1.2.5 Pressure-induced out-of-plane instability

As indicated earlier, in the case of big drape thermoforming, the change of the sheet's geometry during the heating stage is connected with local variations of the distance and the orientation between the exposed zones of the thermoplastic sheet and the infra-red heating element. Hence, it is normal practice to counteract the drooping. Following the heating cycle, pressurized air is pushed from the bottom of the sheet to gently inflate and

flatten it. However, unexpected changes in air pressure cause out-of-plane damping oscillations in the sheet [23,54,55], as seen in Figure 10.

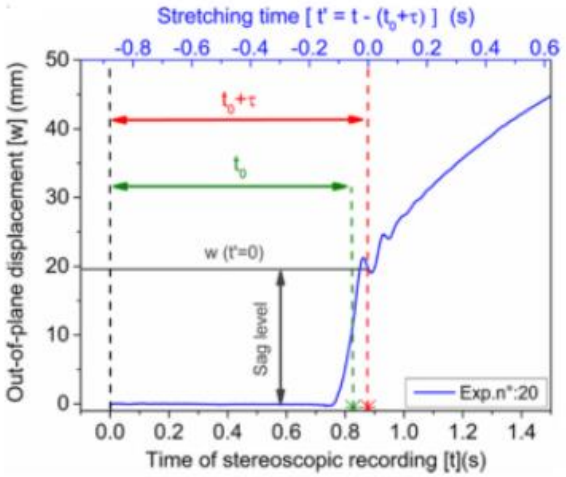

Figure 10: Out-of-plane displacement with oscillations during pre-stretching as a function of time [23]

According to the incomplete list of common thermoforming defects related to plug-assisted thermoforming (refer to section 1.2.1), each flaw can be linked to the corresponding stage of the thermoforming process. Table 2 provides a concise overview of the literature's findings on the most probable occurrence of a fault.

Table 2: Non-extensive overview of thermoforming flaws and their respective considerations in simulation-based studies

Stage	Ref. / Flaws	[56, 57]	[58]	[25] [59]	[54, 55] [34]	[28] [31, 32] [50] [60–62]	[21]	[33] [40]	[20] [39]	[27]	[52]	[63]	[23]
1	Temperature heterogeneity	✓							✓				✓
	Sagging		✓	✓						✓	✓		✓
2	Out-of-plane instability				✓						✓	✓	✓
3	Contact friction (plug-sheet)					✓	✓		✓	✓			
	Non uniform thickness							✓				✓	
Considered Physical formalism		**T**	**M**	**T, M**	**FSI**	**TM**	**TM ***	**TM**	**T, TM ***	**M, TM**	**M, FSI**	**TM , FSI**	**T, FSI**

T = Thermal; M = Mechanical; FSI = Fluid structure interaction; TM = Thermo-mechanical; * = Coupling of thermal and mechanical phenomenon considered.

1.3 Scientific context

1.3.1 Requirement of thermoforming simulations

Process simulation tools are helpful to conduct virtual tests and ascertain different objectives before performing experimental work. A non-extensive overview of studies reporting numerical simulations of thermoforming indicates that such tools are useful to:

(i) Optimize geometric and mechanical parameters of both the process and the product (such as temperature distribution, thickness homogeneity, geometry of the mold, etc.) starting from the design phase in order to minimize the quantity of used materials [61].

(ii) (ii) Minimize process-induced flaws based on a defined material and geometry of the mold [64][22].

(iii) (iii) Evaluate the residual constraints and parameters of mechanical performance of the product models in order to take them into account when studying the behavior of the product in service (behavior and appearance).

(iv) (iv) Identify parameters of mechanical models based on inverse-identification approaches relying on experimental data [65].

(v) (v) Control phenomena which take place during shaping such as orientation or crystallization of polymer macromolecules in order to exploit them to increase the performance of the product or eliminate them if necessary [66].

One of the most typical control factors for both product designers and thermoforming operators is obtaining an accurate estimate of the finished product's ultimate thickness ahead of time [67]. Currently, there are several commercial simulation tools available, including T-Sim, Formview, Polyflow, and PAM-FORM. Nevertheless, the precision of the majority of commercial software is limited, particularly when comparing results to experimental data. Typically, computed thicknesses deviate from experimental measurements. One possible explanation for these differences is the intricate nature of the actual experimental conditions that the material is exposed to, compared to the various numerical assumptions made (such as assuming uniform temperature throughout the sheet thickness) that are necessary to reduce computational time. However, the differences are linked to the limited ability to modify or enhance the pre-existing material models in commercial toolboxes. These models are classified as black boxes and cannot be publicly altered. Developing building simulation tools that can surpass these limitations allows thermoforming operators to customize their virtual testing to match the experimental settings used in industry situations. Table 3 presents a comprehensive summary of the different criteria used by authors in the literature when conducting thermoforming simulations.

Table 3: Non-extensive summary of thermoforming simulations and their respective assumptions

Ref.	Process				FEM based simulations						
					Model			Assumptions			Control
	VA	PA	In	Mat.	H	VE	VEP	Mem.	Friction	Formulation	
[68]	✓			ABS	✓			Thin	No slip	T- Lagrangian	Thickness
[52]	✓			ABS	✓			Thin	No slip	T- Lagrangian	Thickness
[34]			✓	PMMA	✓			Thin	No slip	T- Lagrangian	Thickness
[61]			✓	PMMA	✓			Thin	No slip	T- Lagrangian PAM-FORM*	Mesh refinement
[40]		✓		PMMA	✓			Thin	No slip		Thickness
[69]	✓			ABS		✓		Thin	C-fc = 0.25		
[39]				PS		✓		Thin	C-fc = 0.40		Thickness
[32]				HIPS		✓		Thin	C-fc = 0.50	PAM-STAMP*	Thickness
[60]		✓		HIPS					C-fc = 0.70		Thickness
[70]		✓		HIPS		✓			Frictionless		Thickness
[21]		✓		HIPS			✓	Thin	Temperature -dependent	T-Lagrangian	Thickness
[27]		✓		HIPS					Temperature dependent	T-Lagrangian T-SIM *	Thickness
[56]				PET		✓		Thin		T-Lagrangian ThermoFORM*	Stress
[71]			✓	PMMA	✓			Thick		T- Lagrangian	Thickness

VA: Vacuum assisted thermoforming PA: Plug assisted thermoforming In: Inflation assisted thermoforming C-fc: Coulomb's Friction coefficient Mem.: Membrane assumption

H: Hyperelastic model VE: Viscoeleastic model VEP: Visco-elasto-plastic model T-Lagrangian: Total Lagrangian formulation (*): Commercial software : Dark space: Not enough precisions

1.3.2 Introduction to the Finite Element Method in the context of thermoforming

Simulations of massive deformation issues have been increasingly efficient over the last three decades, thanks to advances in numerical modeling and computing capability. The finite element method (FEM) is a popular numerical approach in solid mechanics. It is used to find an approximate solution to the differential equations of motion in complicated geometries. The use of FEM solvers in commercial software provides a dependable computational approach for analyzing a continuous system with any geometry and material characteristics exposed to various sorts of loads.

In general, the FEM is the translation of a continuous system with infinite degrees of freedom into an equivalent, discrete system with approximate geometry and physical attributes but finite degrees of freedom. The level of approximation utilized will determine the correctness of the calculated solution. Such degrees of freedom are connected to external forces (or any other disturbance) using a series of algebraic equations that define the structure's overall equilibrium state. Figure 11 shows a FEM

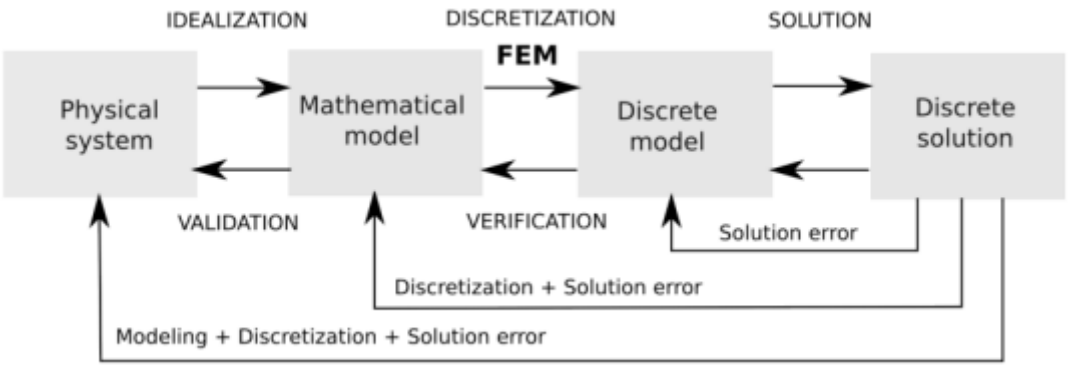

Figure 11: Flowchart of the process followed to find a solution to a problem by means of the FEM [72]

flowchart for solving a basic engineering problem.

The flowchart in Figure 11 depicts: (i) the formulation of the problem into variational form by transforming the differential equations of moments balance into scalar integral equations known as the weak form, and (ii) finite element discretization of the formulation to approximate the exact solution, with each element consisting of a discrete number of points known as nodes. (iii) The discretized algebraic equations are then integrated to fulfill the equation of motion at discrete time intervals using various time integration methods [1].

FEM has a twofold benefit that is quite useful for thermoforming. For starters, it does not prefer any certain shape of the body undergoing deformation, hence it is not limited to one type. Second, it allows for the simulation of enormous strains/deformations in highly nonlinear materials using rigorous formulas, which improves accuracy. As a result, a finite element simulation of thermoforming often has three problem definitions. The first step is to formulate the boundary value issue, which entails specifying the thermomechanical boundary conditions or constraints at the start and end of the time period during which the process occurs. The second step is to define the components, or

type, into which the entire body will be discretized. This is widely known as the meshing procedure. Finally, the material attributes must be included into the numerical model that leads the simulation in estimating the deformability of this particular material under the specified boundary conditions [73]. Mechanical models defining the material's constitutive behavior are therefore integrated in each constituent. This completes all components of the issue specification, allowing a finite element (FE) solution to be initiated [74].

The finite element solution allows the user to discretize components into shell or plate elements. The primary distinction resides in the fact that shell elements are simulated without accounting for the precise thickness of each element, whereas plate components require a thickness value for each individual section. Shell elements do not consider variables such as resistance to bending in the through-plane direction, shearing in the transverse direction, and changes in stresses that occur out-of-plane through the thickness. This is extremely suitable for narrow gauge thermoforming. Thermoplastic sheets can be shaped into a membrane made up of shell fragments, whereas thick gauge thermoforming entails producing a thick sheet utilizing plate components.

1.3.3 Thin membrane-based formulations

The key assumption when treating a thermoplastic sheet as a membrane is that the sheet's thickness is small in comparison to its other in-plane dimensions (length and breadth) [1]. This assumption is plausible since the effects of through-plane bending are minor in most thermoforming simulations (save at the edges near the clamps). In a membrane assumption, the thickness variation across the thermoforming component is estimated while the sheets are assumed to be incompressible [75]. By adding the displacement vector to the reference configuration, the position vectors of each element are updated. The reference configuration might be either the initial configuration at the beginning of time or the ultimate configuration at each time step. The first formulation is referred to as the Total Lagrangian, whereas the second one is known as the Updated Lagrangian. Due to the well-defined initial boundary conditions and reference configuration in thermoforming, the Total Lagrangian formulation is commonly preferred.

The magnitude of the deformation increments decreases iteratively as the solution to the finite element problem approaches convergence, until they reach a threshold value, at which time the simulation is said to be finished. In vacuum or negative thermoforming, less or no movement is anticipated when the sheet makes contact with the mold throughout the process. Convergence happens when every node of the sheet comes into contact with the surface of the mold. In order to replicate the no-slip situation, a node is specifically engineered to be securely fixed in place as soon as it comes into contact with the surface of the mold.

1.3.4 Thick sheet based formulations

Thick sheet formulae do not consider thickness to be trivial, therefore the impacts of bending resistance, through-thickness stress and strain fluctuations, temperature gradient, and so on cannot be overlooked [1,71]. also represents the sheets more accurately, but also adds to the problem's complexity. Unlike its membrane equivalent, a straightforward assumption of incompressibility cannot be made in the case of thick sheets and must be enforced manually using an additional constraint. Furthermore, because stress, strain, and temperature change across the thickness of the element, the FEM issue is inherently more difficult than membrane formulation. The thick sheet formulations can take localized phenomena into account, such as the stress concentrations near the plug and sheet boundary, bending near the clamps, etc. However, these have a minor effect on the actual sheet, and hence it is deemed unnecessary to conduct such a complex formulation in order to save computational time and cost [34].

1.3.5 Material constitutive laws

On a scientific level, modeling thin thermoplastic sheets undergoing thermoforming necessitates a thorough understanding of the material constitutive laws. They are characterized as a material's regulating relations that determine its macroscopic response to external pressures [76]. Such rules must obey thermodynamic principles, particularly the second one, while also meeting the constraints of material frame indifference and the Drucker stability criterion [77].

Constitutive laws take into account the specific entropy and free energy of a deforming body by considering that the work done by the stresses in the body must always be equal to or greater than the rate of change of its free energy for any type of deformation (tension, compression, shear, or twisting) [76,78]. In thermoforming, for example, there is a strong coupling between the thermal constitutive laws that govern the transition of the polymer from glassy solid-state to viscous rubbery state and the mechanical constitutive laws that govern stresses generated at large deformations [62,79]. Typically, these coupling rules are explained using models that eventually determine how a material behaves when specific boundary conditions and an applied load (such as strain or pressure) are present.

Constitutive laws consider the specific entropy and free energy of a deforming body, assuming that the work done by the stresses in the body is always equal to or greater than the rate of change of its free energy for any type of deformation (tension, compression, shear, or twisting) [76,78]. In thermoforming, for example, there is a strong link between the thermal constitutive laws that regulate the polymer's transition from a glassy solid to a viscous rubbery state and the mechanical constitutive laws that govern stresses created by massive deformations [62, 79]. Models often dictate the coupling rules, which ultimately govern the behavior of the material under preset boundary conditions and an applied load, such as strain or pressure.

There are generally two sorts of mechanical models for materials: phenomenological models and physically based models. Phenomenological models prioritize the overall macroscopic response of a material, such as the mathematical representation of strain energy during deformation, rather than changes in its structure. Physically-based models, on the other hand, use some statistical approaches to connect the material's macroscopic reaction to the physics associated with structural changes happening at smaller scales (such as variations in crystallinity or changes in polymer chain orientations) [80]. Within the realm of amorphous thermoplastic simulations, the literature demonstrates that various mechanical models, such as hyperelastic, viscoelastic, or visco-elastoplastic, can be employed for the same material.

1.3.5.1 Thickness homogeneity as an output control parameter

As shown in Table 3, one of the most commonly reported control factors for the accuracy of thermoforming simulations is obtaining the final thickness distribution throughout the

product, which impacts the resilience and material qualities of the completed product [13]. It is recognized as the key criterion for quality control in thermoformed parts [81]. Excluding the accurate model parameters from the simulation will result in inaccurate deformation profile and thickness distribution.

Many authors have examined the influence of process factors on thickness [5, 27, 50], as well as the efficacy of models in estimating the thickness distribution of a thermoformed component [22, 40, 56, 61, 67, 81-83]. This exemplifies the imperative of maintaining a consistent thickness distribution in a thermoformed product.

1.4 Critical discussion and positioning of the current study

It is common in the literature to make plausible assumptions (such as properly clamped edges, nonslipping contact, temperature homogeneity, etc.) for phases that have not been thoroughly investigated in the research. Several limitations of thermoforming simulations have been identified based on prior research findings.

First, it is difficult to assign "real" material and "real" process-specific characteristics to a thermoforming simulation. There is no established approach to help a user build a relationship between the actual parameters that occur in reality and the ones utilized in simulation software [22]. Conventional testing methods provide challenges when it comes to quantifying material properties like compressibility and residual stresses. Consequently, numerous studies assume that the sheet exhibits the characteristics of being incompressible and isotropic. This assumption will also be recognized in the upcoming study. However, the basic assumptions may be challenged by process-induced faults, such as uneven temperature distribution and instability generated by pressure. Similarly, the simulation presupposes that process-specific parameters, such as the duration of heating and the level of air pressure applied, are functioning at optimal efficiency. Nevertheless, it is crucial to acknowledge that these elements may differ in actuality among various thermoforming equipment.

Furthermore, the current commercial thermoforming simulation software operates like black boxes, as it lacks the capability for users to customize the simulation parameters according to their individual needs. Although these software programs simplify the problem to make it understandable for most thermoforming operators, they often rely on

unrealistic thermoforming parameters. Factors such as pressure instability, uneven temperature distribution, and heater efficiency are not taken into account, leading to a departure from the observed results in the real scenario. In addition, the material is depicted using a limited number of established constitutive models from its material database, which restricts the user's capacity to incorporate new models from the existing literature. Conventional thermoforming simulation software is unable to completely replicate the experimental results due to the uniqueness of each piece of thermoforming equipment in relation to the product being manufactured. Each thermoforming application/machinery ideally necessitates specific equipment instrumentation, enabling the user to obtain more precise information about their process parameters. This information can then be adjusted and applied in a finite element model.

As previously mentioned, the thermoforming process is a complex matter involving multiple physical factors. It often includes the combination of two events, such as the stage where something is formed using heat and mechanical forces, or the step where something is stretched before it interacts with a fluid. Consequently, it is challenging to incorporate a complete comprehension of how various physical processes interact with each other and collectively impact the inherent properties of the sheet material inside a single modeling program. An alternative approach that is more dependable involves treating each thermoforming process as an individual entity and constructing a thorough numerical model that considers all of the physical occurrences involved. After the numerical blocks have been completed, the issue can be viewed as a sequential simulation process, where the blocks are connected in a series and the results are transferred. Table 4 provides a concise overview of the fundamental principles of the thermoforming processes.

This study will analyze and explore the process of forming in the context of numerical tool production. An important challenge faced during the modeling of this technique is the existence of uncontrolled boundary conditions at the beginning of the phase, which are often disregarded and ideal conditions are assumed. The thermal boundary circumstances, characterized by a heterogeneous temperature distribution, as well as the structural conditions, such as sheet sagging, have a notably substantial effect on the resulting deformed sheet. This impact is undeniable and encompasses changes in both shape and thickness distribution.

In the thermoforming die market, numerous issues arise that compromise the quality of the desired output and result in energy inefficiencies, leading to excessive production costs. This study specifically concentrates on the air blowing procedure employed in the forming process.

Having conducted extensive study and acquired a wealth of expertise, we now want to investigate the impact of creating molding equipment. There are numerous issues that have a detrimental impact on output. The material is molded by the male and female die in a region where a combination of air blowing and vacuum processes are used. These processes are applied by the male and female tools respectively to achieve a smooth surface and required level of detail in the final product.
The air channel's design causes air flow to pass through the male tool, resulting in air pressure losses and imbalances when it blows onto the target product. We want to modify the configuration of these channels and enhance the balance of the airflow directed onto the product, with the objective of obtaining a greater quantity of finely processed product.

2. MATERIAL AND METHOD

2.1 Expression of the thermoforming process

At first, the procedure of the thermoforming process generally includes three phases; material forming, trimming, and aligning. In order to shape the material, it needs to heat by the resistance and then forming by the male and female tools. In this very operation, air blown onto product and it is vacuumed by the male tool. Then products is cut by blades to seperate from each other, at last, they are arranged in a certain order by the last tool.

Figure 12: Thermoform die machine; forming parts

Figure 13: Thermoform die; closed form

During the forming process, the product is shaped by the male and female tool moving up and down. When the tools fully closed or in other words they fully approach each other, our product is shaped by these tools. It is basically showed in Figure 14.

2.2 Designing thermoform die on Solidworks

In order to better understand we need to draw the forming station including all parts on Solidworks. The analysis will be focus on the top part of the male tool. Drawing the station via a CAD programme gives us a lot of chance to examine and obtain good results and also provides us finding new and creative solutions for problems. It also provides us to increase the working efficieny, minimize the energy consumptions and production costs.

Figure 14: Basic representation of the male and female die

We draw all of the thermoform machine parts on solidworks in order to understand the way of its working principle and get more idea to how does air get distribute to products and how it affects the shaipng.

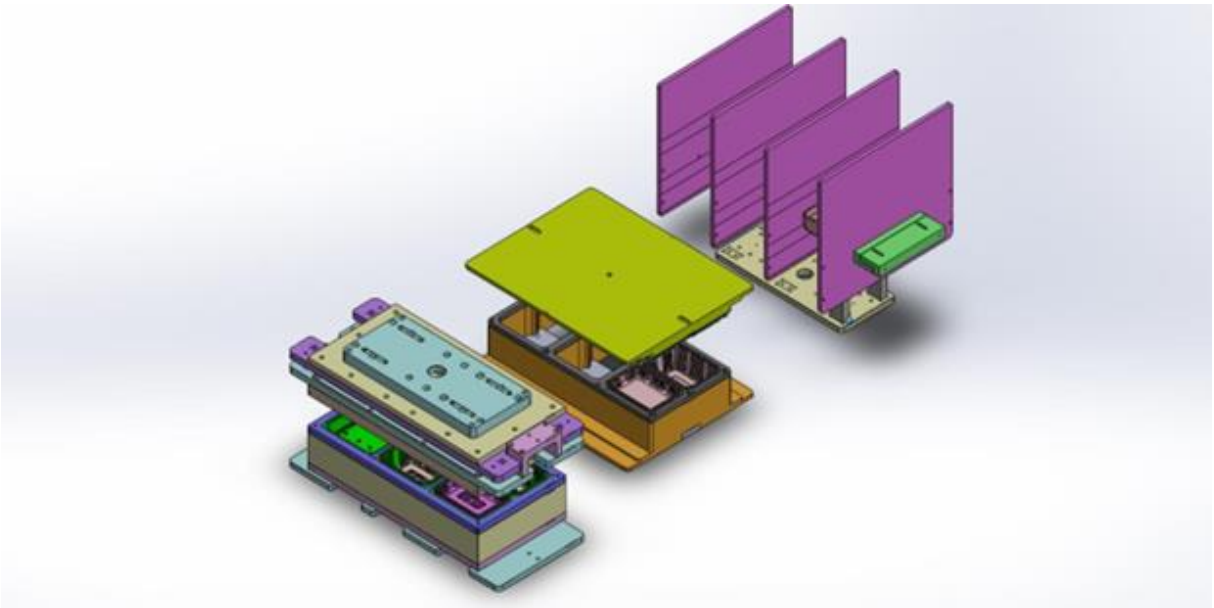

Figure 15: Three-cavity bowl-lid mold drawings on Solidworks

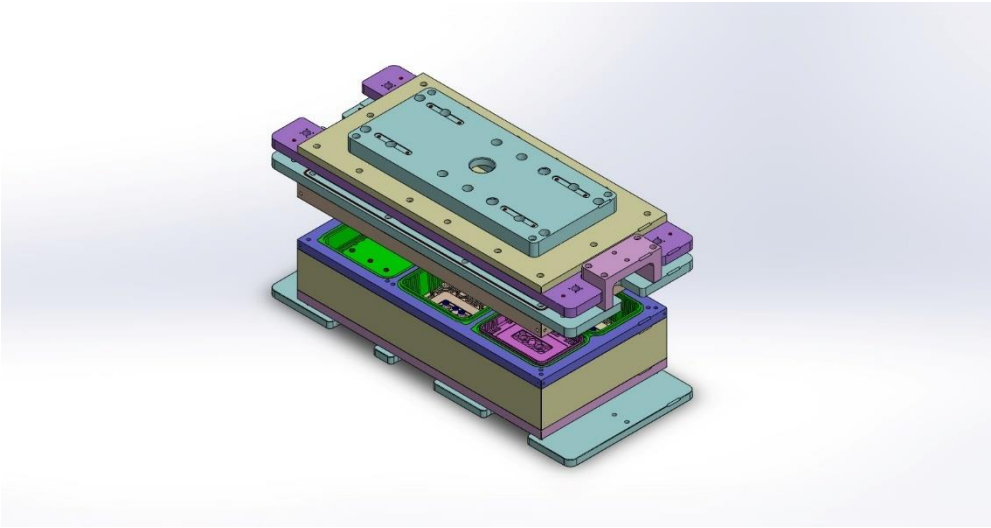

Figure 16: Forming station

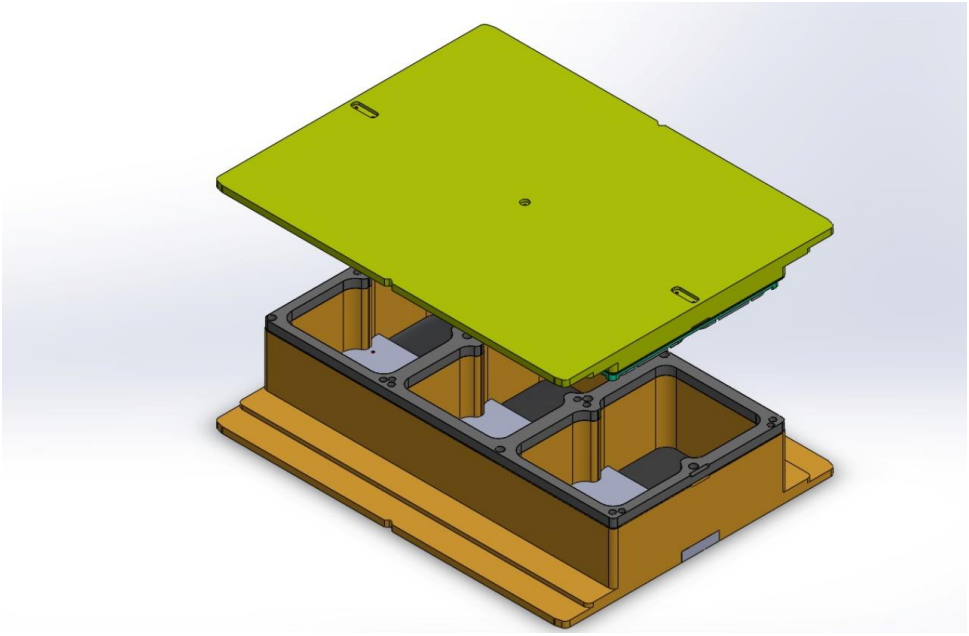

Figure 17: Cutting station

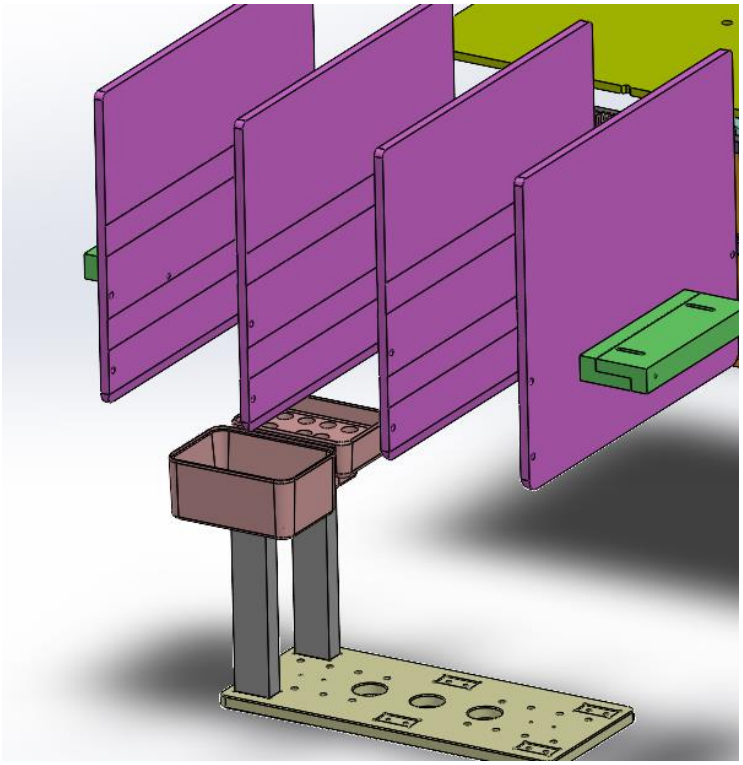

Figure 18: Stacking station

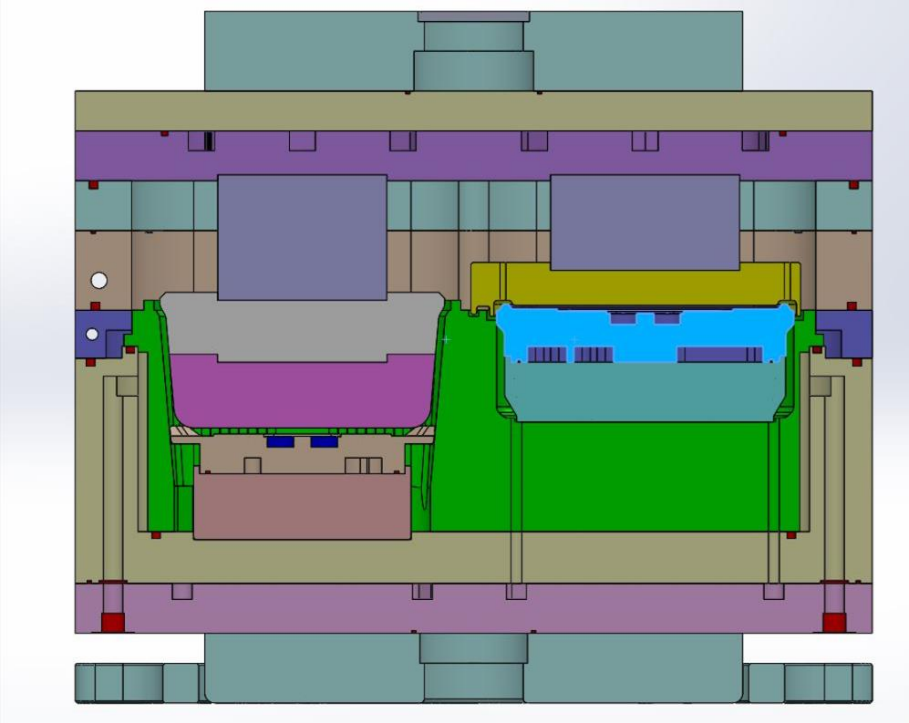

Figure 19: The section view of the forming station from other side

If we take a look at the process that we investigate, the section view of our forming station will helps us sufficiently as shown in Figure 19. Suppose certain amount of air is given into system through the hole at the top and begins to be distributed through channels inside this station.

When it reaches the product, it creates a pressure to product's surface and allows the product to take the shape of the mold better. In the Figure 19 the product is between the green and pink part of the assembly if we make a clear expression.

All of these process in other words the production of the desired material generated in approximately 3-4 seconds then arranged at last. These stations have high integration and interference while working together.

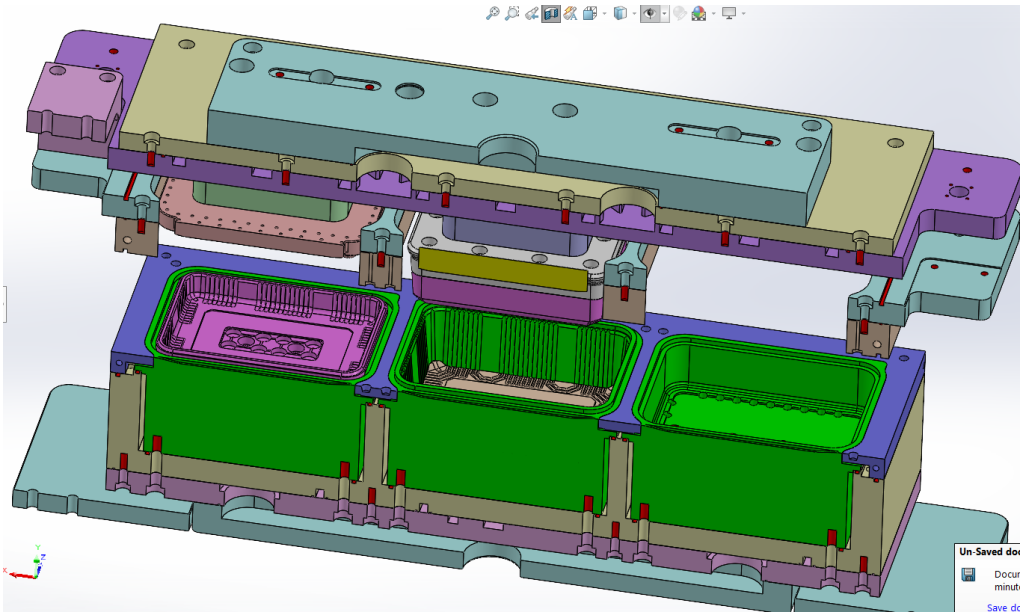

Figure 20: The section view of forming station

Air is blown into system from the top hole of the assembly as shown in Figure 16. Generally the air channel are produced same certain standard in this part. Air is at first pass through the part shown in the Figure 20, our reviews start in here because the distribution of the air occurs at this very place. All of the holes are for fasteners except bigger one. Air is given into system through this hole, when it reaches the last part that we desire to analyze, air is distributed through this part's hole (purple one of top part).

2.3 Plastics thermoforming: Thermoplastics in engineering

Today, plastics are the most versatile material for consumer and engineering application. In a volume basis, the plastics are more used than metals. The materials used above the barrier of 1Mton $year^{-1}$ in the major markets (Europe, the United States, Canada and Japan) are only a handful, and they include polypropylene (PP) and low density polyethylene (LDPE), mostly used in packacing; poly vinyl chloride (PVC) applied in piping; and finally high density polyethylene (HDPE) and polyethylene terephtalate (PET) which overccame polystyrene (PS) due to its increasing usage in the packaging of carbonated drinks [39].

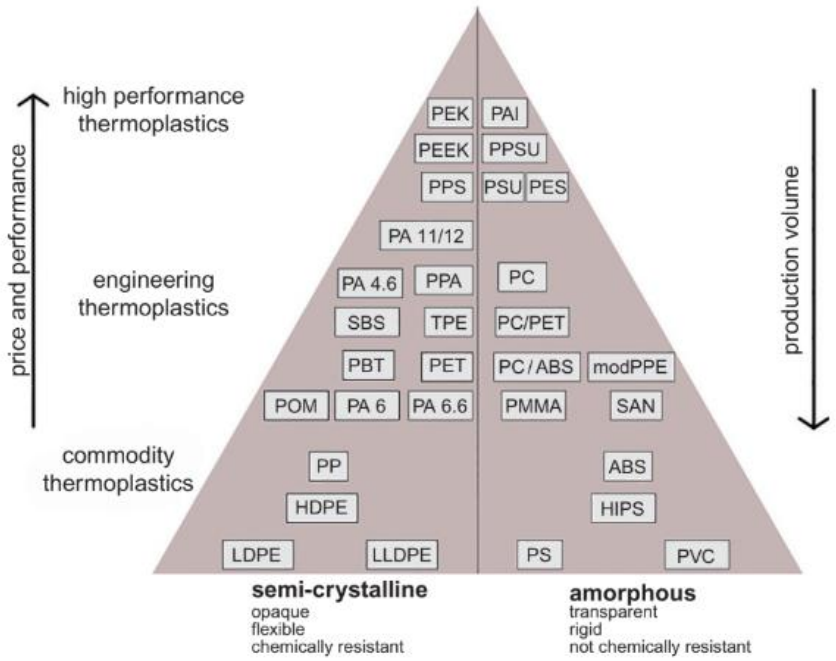

Figure 21: A comparison of commodity plastics, engineering plastics, and high-performance plastics.

It is known that thermoplastics have huge amount of area of our life. Almost every packaged product in the supermarkets, every beverage we drink, every carrier bag to carry the products we buy from market and another thousands of examples like these are produced from thermoplastics. In this study, our product that we desire to investigate is made from polyethylene terephtalate (PET). It is good to take a look of material property

of PET to understand why it is used in our daily life commonly and in order to analyze our product we need to know important characteristic properties abut PET.

2.4 Polyethylene terephtalate

One such flexible linear semicrystalline thermoplastic is polyethylene terephthalate, most commonly known as PET or PETE. It belongs to the class of polymers known as polyester. Because of their unique combination of properties, these resins are well-known. Mechanical, thermal, and chemical resistance, along with dimensional stability, are some of these features. Citric acid (10H8O4)n is the chemical formula.

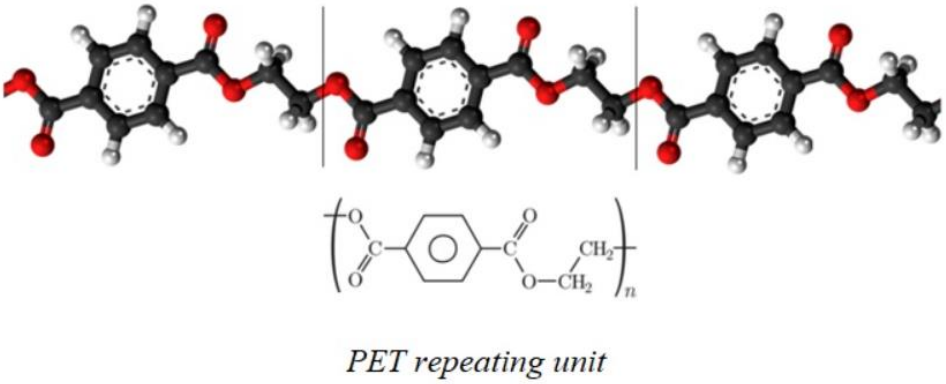

Figure 22: Molecular Structure of Polyethylene Terephthalate

2.4.1 What properties assist in PET selection

Polyethylene terephthalate, when left unprocessed, is a semi-crystalline resin that is extremely malleable and colorless. It can be semi-rigid or stiff, depending on the treatment. In addition to being impact-, moisture-, alcohol-, and solvent-resistant, it possesses outstanding dimensional stability.

Key benefits:

-Include higher strength, heat distortion temperature (HDT), and stiffness compared to PBT.

-Very sturdy and lightweight, and hence easy and efficient to carry.

-Excellent gas (oxygen, carbon dioxide) and moisture barrier characteristics.

-Excellent electrical insulation qualities.

-Temperature range: -60 to 130°C.

-Low gas permeability, especially with CO2.

-Suitable for transparent applications, when quenched during processing.

-It does not break or fracture. It is essentially shatter-resistant and hence a potential glass alternative in several applications.

-It is recyclable and microwave radiation

-The FDA, Health Canada, the European Food Safety Authority, and other health organizations have all cleared it for interaction with foods and drinks. PET grades that are acceptable for food contact.
Chemical characteristics: modest resistance to diluted acids, oils, grease, aliphatic hydrocarbons, and alcohols.

The degree of crystallinity determines the glass transition temperature of PET, which can vary. A temperature range of 65 to 80 degrees Celsius is described for it. A temperature range of 240–270°C is its melting point. Tg for amorphous PET is 65°C. As the degree of crystallinity rises, the Tg also increases.

Crystallization occurs with a maximum crystallization rate of 178°C at:

-the temperature range of 10°C above its Tg, and

-up to 10°C below its melting temperature.

It normally reaches a crystallinity of 40-50%. It can also be polymerized to a co-polymer that cannot crystallize.

2.4.2 Limitations of PET

PET has greatly improved our daily lives, however there are still some downsides to the material.

The crystallized form of PET has:

-lower impact

-lower moldability

Because of its relatively slow crystallization rate, these qualities are inferior to those of PBT. In addition, powerful bases, alkalis, and boiling water have little trouble affecting PET while it is in its amorphous state. It is readily affected by aromatic and chlorinated hydrocarbons, ketones, and diluted acids and bases at high temperatures (>60°C). Crystalline PET polyester is a common molding material because it can handle:

-aggressive chemical environment as well as

-elevated temperatures

According to these datas PET is the best suitable material for food packaging in thermoforming.

The chemical and physical properties of PET are widely used in the thermoforming molding market. When heated, it becomes ductile, making it easier to work, and when cooled, it becomes harder, making it suitable for daily use.

Table 4: Intrinsic properties of PET polymers [85]

Property	**Value (unit)**
Average molecular weight	30,000-80,000 g mol^{-1}
Density	1.41 g cm^3
Melting temperature	255-265 ℃
Young's modulus	1700 Mpa
Water absorption	0.5%

Our product is commonly used in food packaging known as lid and cup and it is made from PET. It is widely used in the packaging of many food materials, in the packaging of grained vegetables and fruits, and in the packaging of many other products such as nuts and legumes.

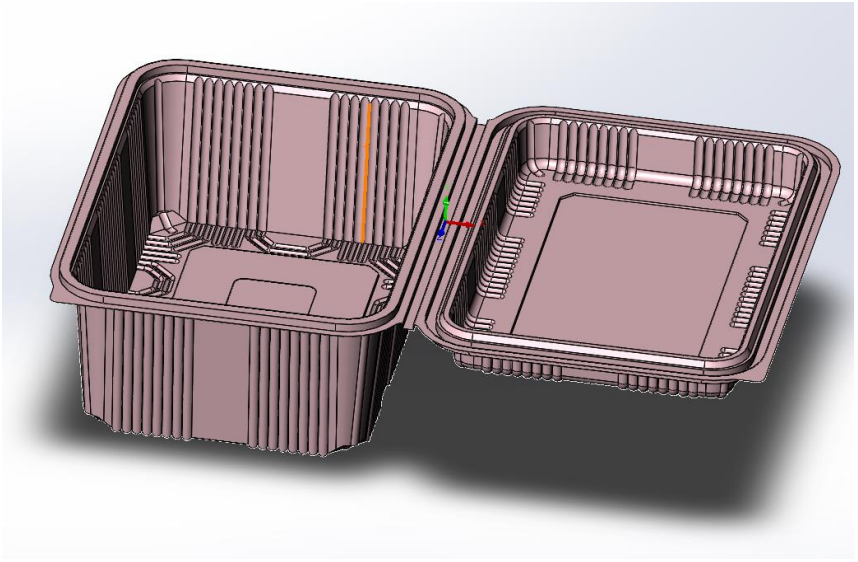

Figure 23: Lid bowl pot made from PET

3. RESULTS and DISCUSSION

To understand the intended analysis and simulation here is small brief about process; As soon as the PET product in roll is heated and reaches the forming station, the male and female molds interlock to provide the product shape. At this very moment the air blown into assemble in Figure 25. The air flow through this part reachs the material and stick it to the female mold at the bottom part. But the problem start in here because in thermoforming market, the air channels of this part is not important for the producer. Thus, they can not see the difference between optimization of these channels and the standard ones.

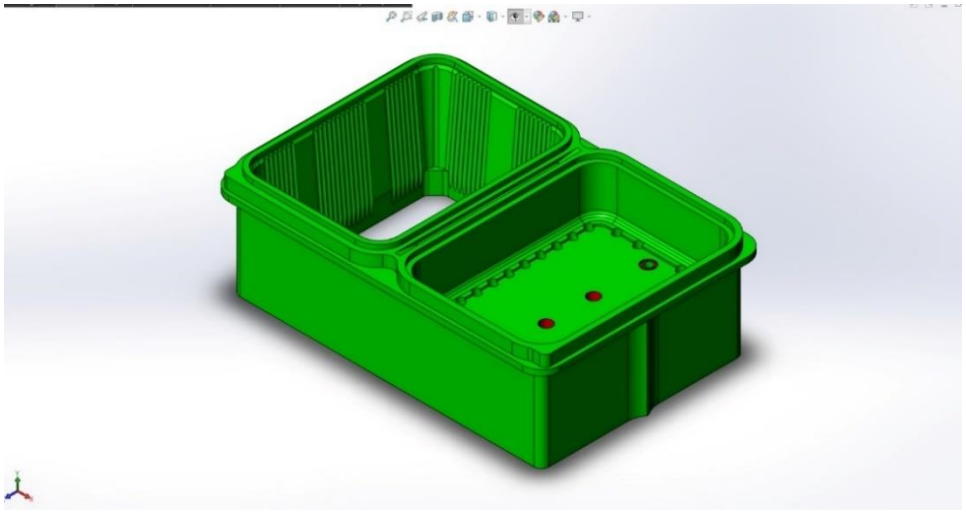

Figure 24: Female mold that gives the product's shape

Figure 25: PET coil

3.1 Investigating the standard design of air channels

The PET material heating by the resistance on the forming station, when it is heated it is easy to reshape this material. Unfortunately, it is not enough for the give an exact shape to this material by the female mold. In addition to forming, there are air blowing and vacuuming process to get more fine product.

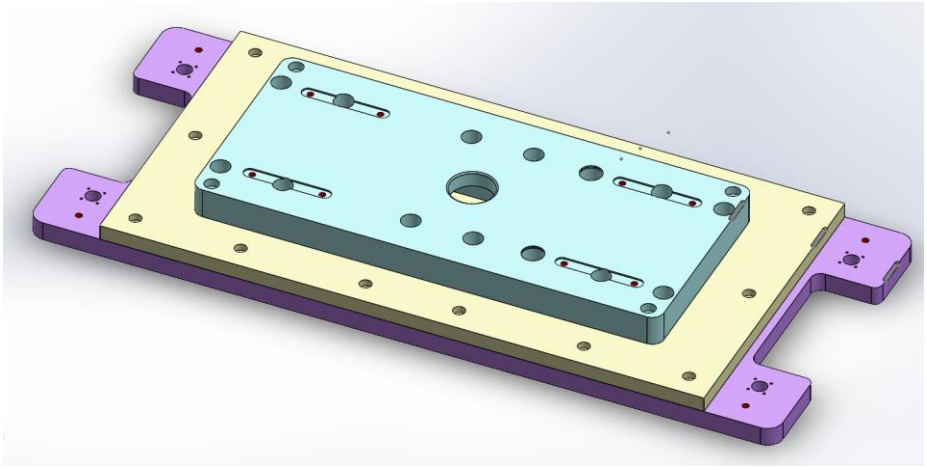

Figure 26: Top part of female mold

To avoid an any confuse during analysis and get better solutions, we can ignore the fastener holes. The system must be closed for CFD analysis because we choose air inlet and outlet then any other openings may creates confusion. We desire to make CFD analysis on this material through its channels because we know that in our country, Turkey, thermoform molding markets generally use same standards, same production methods and tools approximately. We know very well that mostly the effects of air channels in this part to the product are not taken into account. Our desire in here is to build up and change the design of air channels based on some basic fluid mechanics knowledge.

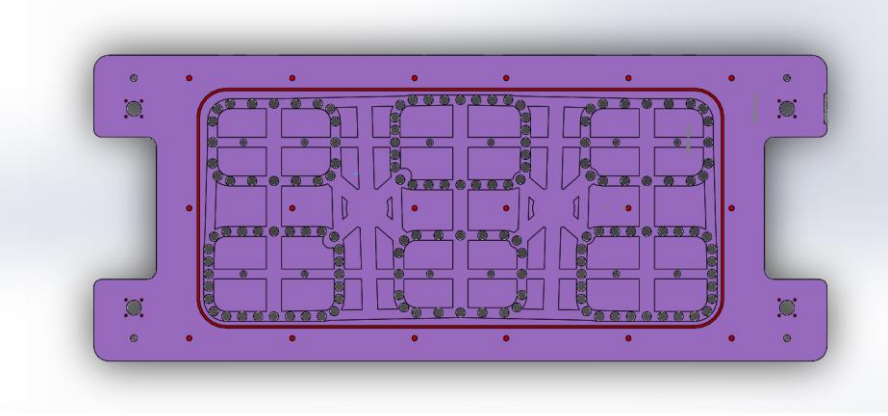

Figure 27: The standard design of air channels before we have changed it

The holes have 12 mm diameter of each. To molding one piece of lid and cup, there is one group of hole assemble. We can think that one side is for the lid and other one is for

the cup. Our exact goal is to distribute the air equally through these holes. At first, we analyze the standard shape of air channels seen in Figure 27.

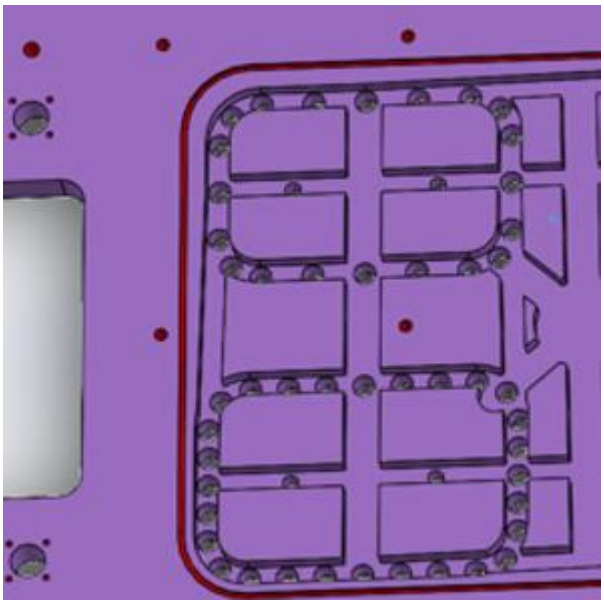

Figure 28: One group of holes

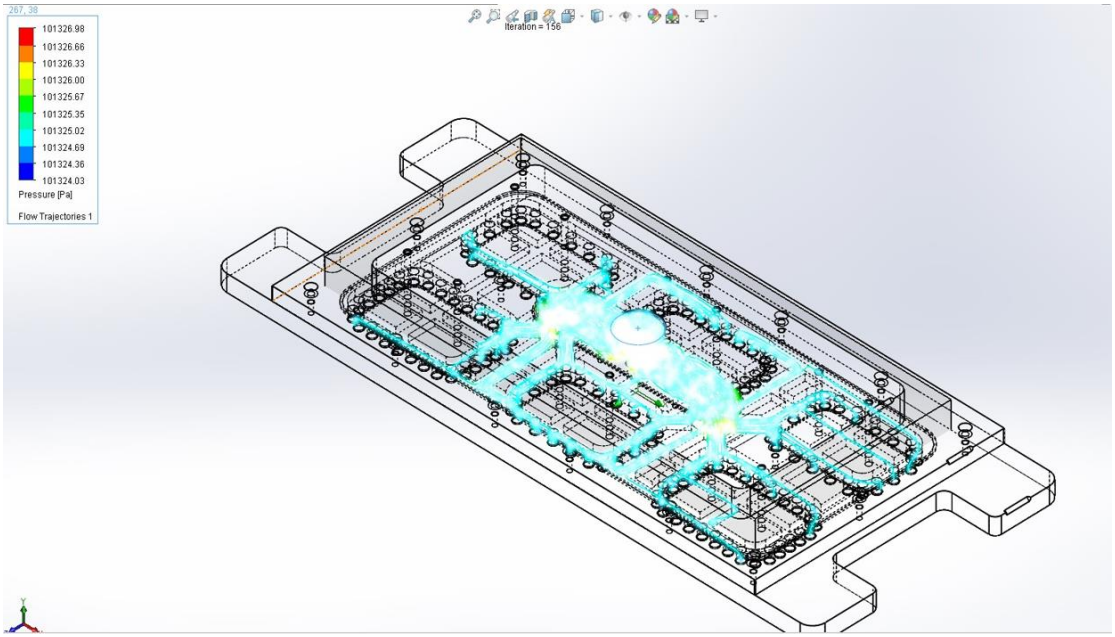

Figure 29: Air flow analysis of standard shape channel using Solidworks

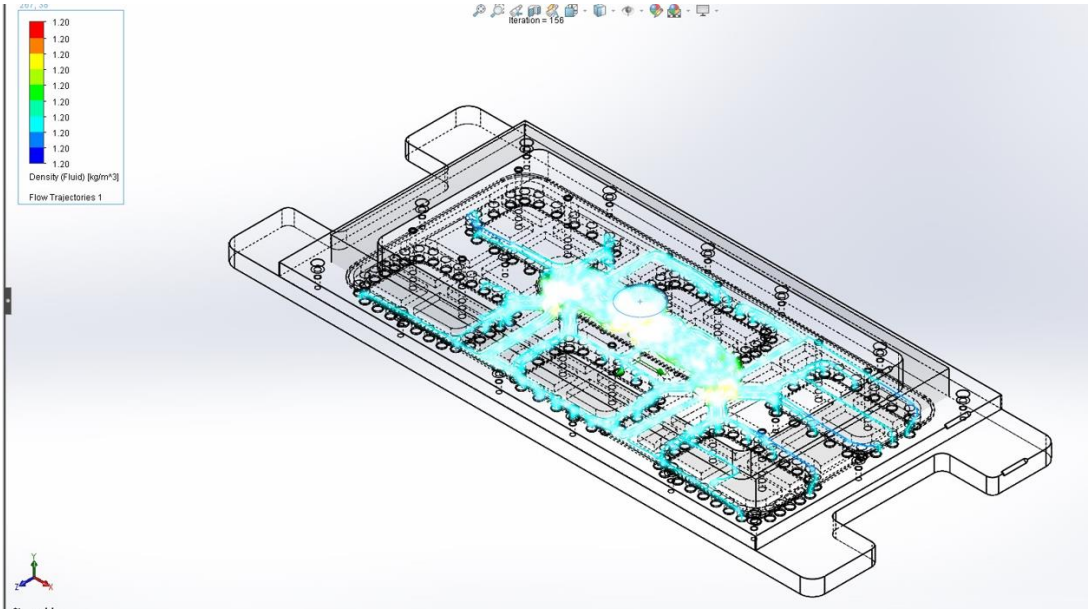

Figure 30: Air flow analysis of standard shape channel using Solidworks

As we see in Figure 29 and Figure 30, air is not equally distributed through this channel. We see that the main problem in here is the shape of these channel. According to basic fluid mechanics knowledge, let us consider a pipe that has no curve and no recession, air flows through this pipe smoothly if we compare to other curved pipes. We thought that the more curve-free we designed the channels, the more evenly we could distribute the air to the holes, and we modeled this.

We have 144 holes totally on the standard part and reaches the results of each hole for volumetric flow. Our input volume flow rate is 120 lt/min of air.

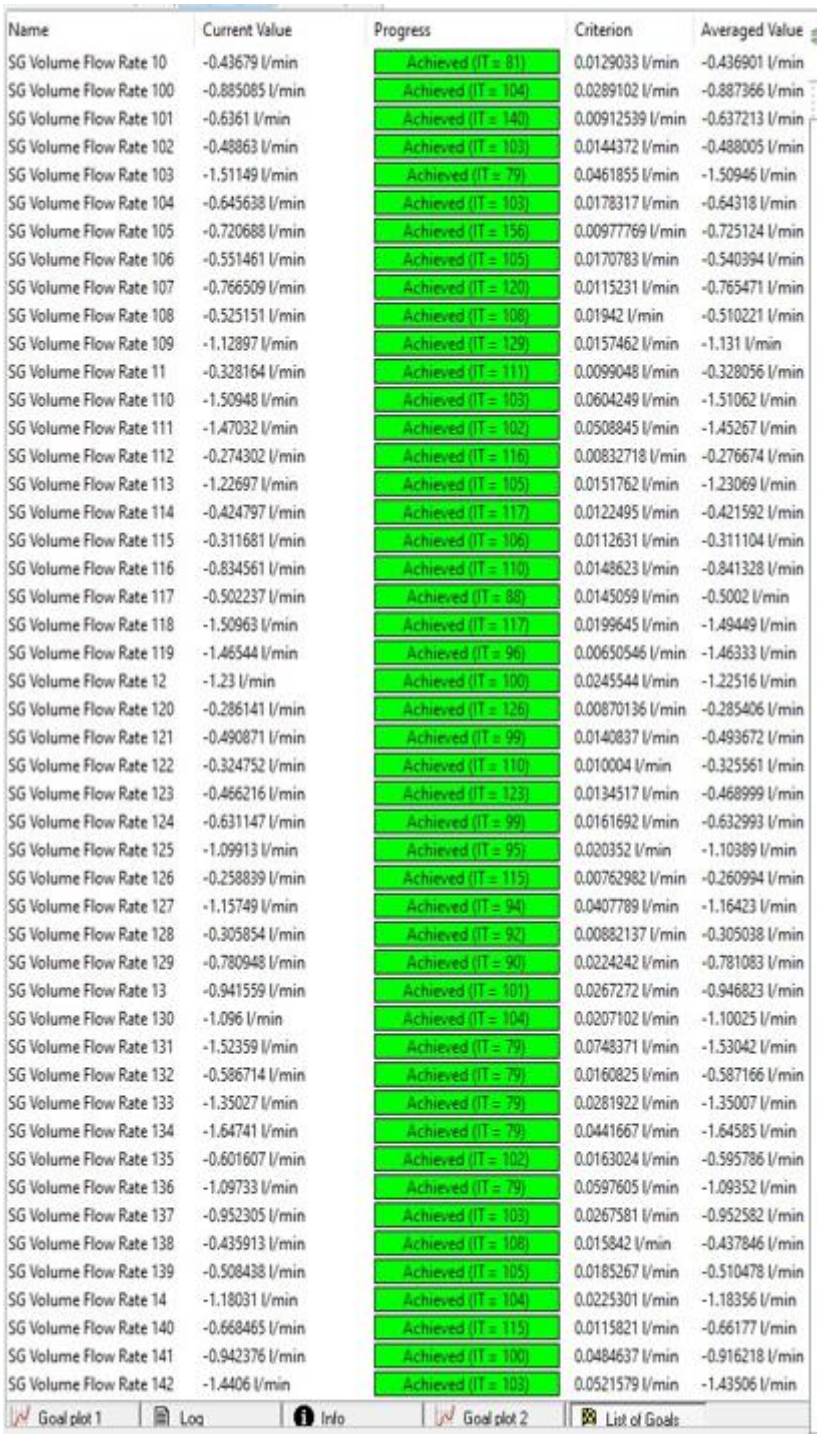

Name	Current Value	Progress	Criterion	Averaged Value
SG Volume Flow Rate 10	-0.43679 l/min	Achieved (IT = 81)	0.0129033 l/min	-0.436901 l/min
SG Volume Flow Rate 100	-0.885085 l/min	Achieved (IT = 104)	0.0289102 l/min	-0.887366 l/min
SG Volume Flow Rate 101	-0.6361 l/min	Achieved (IT = 140)	0.00912539 l/min	-0.637213 l/min
SG Volume Flow Rate 102	-0.48863 l/min	Achieved (IT = 103)	0.0144372 l/min	-0.488005 l/min
SG Volume Flow Rate 103	-1.51149 l/min	Achieved (IT = 79)	0.0461855 l/min	-1.50946 l/min
SG Volume Flow Rate 104	-0.645638 l/min	Achieved (IT = 103)	0.0178317 l/min	-0.64318 l/min
SG Volume Flow Rate 105	-0.720688 l/min	Achieved (IT = 156)	0.00977769 l/min	-0.725124 l/min
SG Volume Flow Rate 106	-0.551461 l/min	Achieved (IT = 105)	0.0170783 l/min	-0.540394 l/min
SG Volume Flow Rate 107	-0.766509 l/min	Achieved (IT = 120)	0.0115231 l/min	-0.765471 l/min
SG Volume Flow Rate 108	-0.525151 l/min	Achieved (IT = 108)	0.01942 l/min	-0.510221 l/min
SG Volume Flow Rate 109	-1.12897 l/min	Achieved (IT = 129)	0.0157462 l/min	-1.131 l/min
SG Volume Flow Rate 11	-0.328164 l/min	Achieved (IT = 111)	0.0099048 l/min	-0.328056 l/min
SG Volume Flow Rate 110	-1.50948 l/min	Achieved (IT = 103)	0.0604249 l/min	-1.51062 l/min
SG Volume Flow Rate 111	-1.47032 l/min	Achieved (IT = 102)	0.0508845 l/min	-1.45267 l/min
SG Volume Flow Rate 112	-0.274302 l/min	Achieved (IT = 116)	0.00832718 l/min	-0.276674 l/min
SG Volume Flow Rate 113	-1.22697 l/min	Achieved (IT = 105)	0.0151762 l/min	-1.23069 l/min
SG Volume Flow Rate 114	-0.424797 l/min	Achieved (IT = 117)	0.0122495 l/min	-0.421592 l/min
SG Volume Flow Rate 115	-0.311681 l/min	Achieved (IT = 106)	0.0112631 l/min	-0.311104 l/min
SG Volume Flow Rate 116	-0.834561 l/min	Achieved (IT = 110)	0.0148623 l/min	-0.841328 l/min
SG Volume Flow Rate 117	-0.502237 l/min	Achieved (IT = 88)	0.0145059 l/min	-0.5002 l/min
SG Volume Flow Rate 118	-1.50963 l/min	Achieved (IT = 117)	0.0199645 l/min	-1.49449 l/min
SG Volume Flow Rate 119	-1.46544 l/min	Achieved (IT = 96)	0.00650546 l/min	-1.46333 l/min
SG Volume Flow Rate 12	-1.23 l/min	Achieved (IT = 100)	0.0245544 l/min	-1.22516 l/min
SG Volume Flow Rate 120	-0.286141 l/min	Achieved (IT = 126)	0.00870136 l/min	-0.285406 l/min
SG Volume Flow Rate 121	-0.490871 l/min	Achieved (IT = 99)	0.0140837 l/min	-0.493672 l/min
SG Volume Flow Rate 122	-0.324752 l/min	Achieved (IT = 110)	0.010004 l/min	-0.325561 l/min
SG Volume Flow Rate 123	-0.466216 l/min	Achieved (IT = 123)	0.0134517 l/min	-0.468999 l/min
SG Volume Flow Rate 124	-0.631147 l/min	Achieved (IT = 99)	0.0161692 l/min	-0.632993 l/min
SG Volume Flow Rate 125	-1.09913 l/min	Achieved (IT = 95)	0.020352 l/min	-1.10389 l/min
SG Volume Flow Rate 126	-0.258839 l/min	Achieved (IT = 115)	0.00762982 l/min	-0.260994 l/min
SG Volume Flow Rate 127	-1.15749 l/min	Achieved (IT = 94)	0.0407789 l/min	-1.16423 l/min
SG Volume Flow Rate 128	-0.305854 l/min	Achieved (IT = 92)	0.00882137 l/min	-0.305038 l/min
SG Volume Flow Rate 129	-0.780948 l/min	Achieved (IT = 90)	0.0224242 l/min	-0.781083 l/min
SG Volume Flow Rate 13	-0.941559 l/min	Achieved (IT = 101)	0.0267272 l/min	-0.946823 l/min
SG Volume Flow Rate 130	-1.096 l/min	Achieved (IT = 104)	0.0207102 l/min	-1.10025 l/min
SG Volume Flow Rate 131	-1.52359 l/min	Achieved (IT = 79)	0.0748371 l/min	-1.53042 l/min
SG Volume Flow Rate 132	-0.586714 l/min	Achieved (IT = 79)	0.0160825 l/min	-0.587166 l/min
SG Volume Flow Rate 133	-1.35027 l/min	Achieved (IT = 79)	0.0281922 l/min	-1.35007 l/min
SG Volume Flow Rate 134	-1.64741 l/min	Achieved (IT = 79)	0.0441667 l/min	-1.64585 l/min
SG Volume Flow Rate 135	-0.601607 l/min	Achieved (IT = 102)	0.0163024 l/min	-0.595786 l/min
SG Volume Flow Rate 136	-1.09733 l/min	Achieved (IT = 79)	0.0597605 l/min	-1.09352 l/min
SG Volume Flow Rate 137	-0.952305 l/min	Achieved (IT = 103)	0.0267581 l/min	-0.952582 l/min
SG Volume Flow Rate 138	-0.435913 l/min	Achieved (IT = 108)	0.015842 l/min	-0.437846 l/min
SG Volume Flow Rate 139	-0.508438 l/min	Achieved (IT = 105)	0.0185267 l/min	-0.510478 l/min
SG Volume Flow Rate 14	-1.18031 l/min	Achieved (IT = 104)	0.0225301 l/min	-1.18356 l/min
SG Volume Flow Rate 140	-0.668465 l/min	Achieved (IT = 115)	0.0115821 l/min	-0.66177 l/min
SG Volume Flow Rate 141	-0.942376 l/min	Achieved (IT = 100)	0.0484637 l/min	-0.916218 l/min
SG Volume Flow Rate 142	-1.4406 l/min	Achieved (IT = 103)	0.0521579 l/min	-1.43506 l/min

Goal plot 1 | Log | Info | Goal plot 2 | List of Goals

Figure 31: Output value of volume flow rate of each hole for standard air channel design

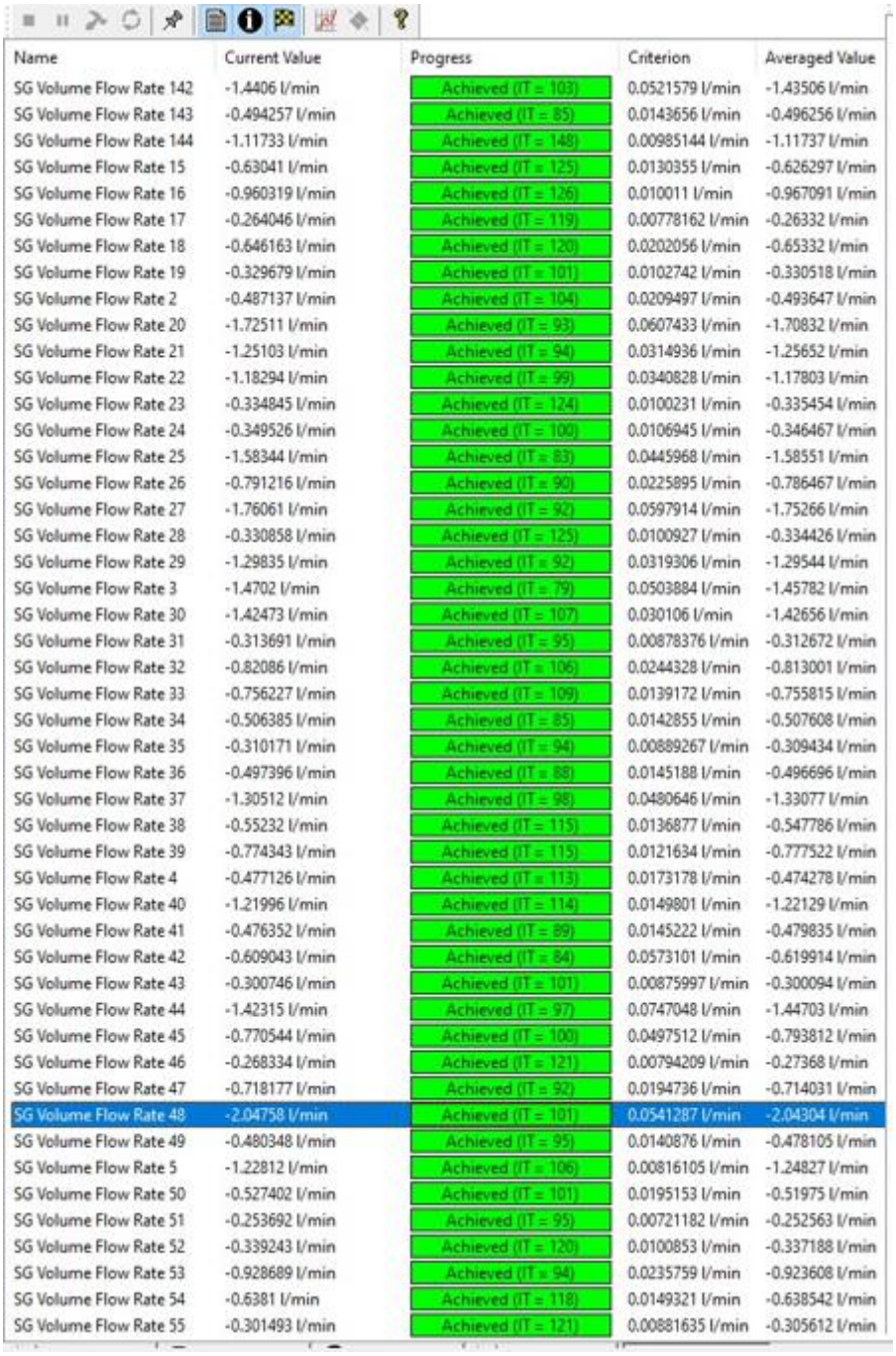

Name	Current Value	Progress	Criterion	Averaged Value
SG Volume Flow Rate 142	-1.4406 l/min	Achieved (IT = 103)	0.0521579 l/min	-1.43506 l/min
SG Volume Flow Rate 143	-0.494257 l/min	Achieved (IT = 85)	0.0143656 l/min	-0.496256 l/min
SG Volume Flow Rate 144	-1.11733 l/min	Achieved (IT = 148)	0.00985144 l/min	-1.11737 l/min
SG Volume Flow Rate 15	-0.63041 l/min	Achieved (IT = 125)	0.0130355 l/min	-0.626297 l/min
SG Volume Flow Rate 16	-0.960319 l/min	Achieved (IT = 126)	0.010011 l/min	-0.967091 l/min
SG Volume Flow Rate 17	-0.264046 l/min	Achieved (IT = 119)	0.00778162 l/min	-0.26332 l/min
SG Volume Flow Rate 18	-0.646163 l/min	Achieved (IT = 120)	0.0202056 l/min	-0.65332 l/min
SG Volume Flow Rate 19	-0.329679 l/min	Achieved (IT = 101)	0.0102742 l/min	-0.330518 l/min
SG Volume Flow Rate 2	-0.487137 l/min	Achieved (IT = 104)	0.0209497 l/min	-0.493647 l/min
SG Volume Flow Rate 20	-1.72511 l/min	Achieved (IT = 93)	0.0607433 l/min	-1.70832 l/min
SG Volume Flow Rate 21	-1.25103 l/min	Achieved (IT = 94)	0.0314936 l/min	-1.25652 l/min
SG Volume Flow Rate 22	-1.18294 l/min	Achieved (IT = 99)	0.0340828 l/min	-1.17803 l/min
SG Volume Flow Rate 23	-0.334845 l/min	Achieved (IT = 124)	0.0100231 l/min	-0.335454 l/min
SG Volume Flow Rate 24	-0.349526 l/min	Achieved (IT = 100)	0.0106945 l/min	-0.346467 l/min
SG Volume Flow Rate 25	-1.58344 l/min	Achieved (IT = 83)	0.0445968 l/min	-1.58551 l/min
SG Volume Flow Rate 26	-0.791216 l/min	Achieved (IT = 90)	0.0225895 l/min	-0.786467 l/min
SG Volume Flow Rate 27	-1.76061 l/min	Achieved (IT = 92)	0.0597914 l/min	-1.75266 l/min
SG Volume Flow Rate 28	-0.330858 l/min	Achieved (IT = 125)	0.0100927 l/min	-0.334426 l/min
SG Volume Flow Rate 29	-1.29835 l/min	Achieved (IT = 92)	0.0319306 l/min	-1.29544 l/min
SG Volume Flow Rate 3	-1.4702 l/min	Achieved (IT = 79)	0.0503884 l/min	-1.45782 l/min
SG Volume Flow Rate 30	-1.42473 l/min	Achieved (IT = 107)	0.030106 l/min	-1.42656 l/min
SG Volume Flow Rate 31	-0.313691 l/min	Achieved (IT = 95)	0.00878376 l/min	-0.312672 l/min
SG Volume Flow Rate 32	-0.82086 l/min	Achieved (IT = 106)	0.0244328 l/min	-0.813001 l/min
SG Volume Flow Rate 33	-0.756227 l/min	Achieved (IT = 109)	0.0139172 l/min	-0.755815 l/min
SG Volume Flow Rate 34	-0.506385 l/min	Achieved (IT = 85)	0.0142855 l/min	-0.507608 l/min
SG Volume Flow Rate 35	-0.310171 l/min	Achieved (IT = 94)	0.00889267 l/min	-0.309434 l/min
SG Volume Flow Rate 36	-0.497396 l/min	Achieved (IT = 88)	0.0145188 l/min	-0.496696 l/min
SG Volume Flow Rate 37	-1.30512 l/min	Achieved (IT = 98)	0.0480646 l/min	-1.33077 l/min
SG Volume Flow Rate 38	-0.55232 l/min	Achieved (IT = 115)	0.0136877 l/min	-0.547786 l/min
SG Volume Flow Rate 39	-0.774343 l/min	Achieved (IT = 115)	0.0121634 l/min	-0.777522 l/min
SG Volume Flow Rate 4	-0.477126 l/min	Achieved (IT = 113)	0.0173178 l/min	-0.474278 l/min
SG Volume Flow Rate 40	-1.21996 l/min	Achieved (IT = 114)	0.0149801 l/min	-1.22129 l/min
SG Volume Flow Rate 41	-0.476352 l/min	Achieved (IT = 89)	0.0145222 l/min	-0.479835 l/min
SG Volume Flow Rate 42	-0.609043 l/min	Achieved (IT = 84)	0.0573101 l/min	-0.619914 l/min
SG Volume Flow Rate 43	-0.300746 l/min	Achieved (IT = 101)	0.00875997 l/min	-0.300094 l/min
SG Volume Flow Rate 44	-1.42315 l/min	Achieved (IT = 97)	0.0747048 l/min	-1.44703 l/min
SG Volume Flow Rate 45	-0.770544 l/min	Achieved (IT = 100)	0.0497512 l/min	-0.793812 l/min
SG Volume Flow Rate 46	-0.268334 l/min	Achieved (IT = 121)	0.00794209 l/min	-0.27368 l/min
SG Volume Flow Rate 47	-0.718177 l/min	Achieved (IT = 92)	0.0194736 l/min	-0.714031 l/min
SG Volume Flow Rate 48	-2.04758 l/min	Achieved (IT = 101)	0.0541287 l/min	-2.04304 l/min
SG Volume Flow Rate 49	-0.480348 l/min	Achieved (IT = 95)	0.0140876 l/min	-0.478105 l/min
SG Volume Flow Rate 5	-1.22812 l/min	Achieved (IT = 106)	0.00816105 l/min	-1.24827 l/min
SG Volume Flow Rate 50	-0.527402 l/min	Achieved (IT = 101)	0.0195153 l/min	-0.51975 l/min
SG Volume Flow Rate 51	-0.253692 l/min	Achieved (IT = 95)	0.00721182 l/min	-0.252563 l/min
SG Volume Flow Rate 52	-0.339243 l/min	Achieved (IT = 120)	0.0100853 l/min	-0.337188 l/min
SG Volume Flow Rate 53	-0.928689 l/min	Achieved (IT = 94)	0.0235759 l/min	-0.923608 l/min
SG Volume Flow Rate 54	-0.6381 l/min	Achieved (IT = 118)	0.0149321 l/min	-0.638542 l/min
SG Volume Flow Rate 55	-0.301493 l/min	Achieved (IT = 121)	0.00881635 l/min	-0.305612 l/min

Figure 32: Output value of volume flow rate of each hole for standard air channel design

We obtain the output volume/flow rate values of each holes for standard air channel design seen in Figure 31 and Figure 32. It can be seen easily that non of holes volume/flow rate is same with each other. The problem in here causes huge amount of air pressure loss, constant energy loss and it reduces the surface quality, wall thikcness of produced

materials. Then we decide to change the design of air channel and again obtain the results to see the difference.

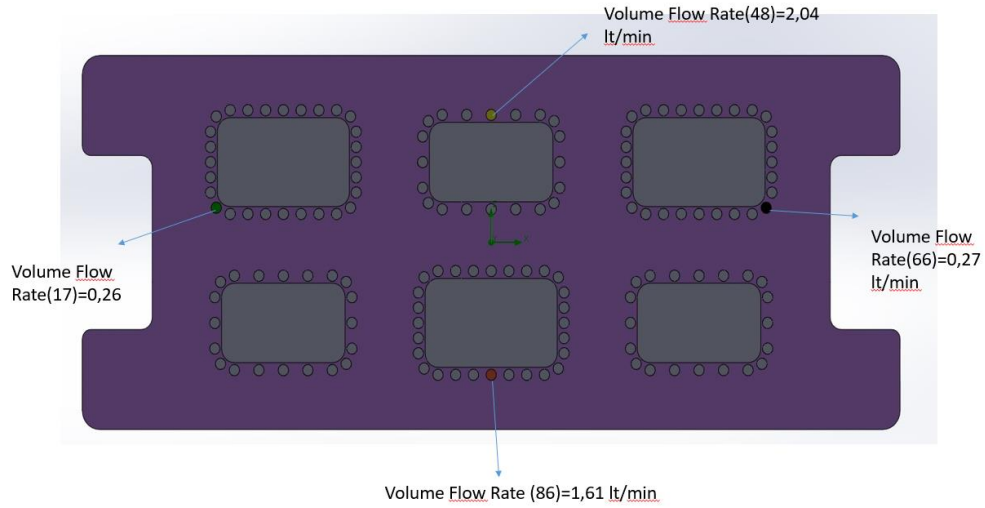

Figure 33: Volume flow rate representation of some holes

As you can see in Figure 33, the air volume/flow rate difference between some specimens are too much. In order to decrease these difference air channel shapes need to be changed.

Table 5: Results of volume flow rate of some holes of standard design

Volume flow rate (17)	**0.25**	**0,20 %**
Volume flow rate (48)	2.04	1,7 %
Volume flow rate (66)	0.27	0,225 %
Volume flow rate (86)	1.61	1,34 %

We have 144 holes of this part. It can be easily calculate the amount of air coming out of each hole;

$$\frac{120\ lt/min}{144} = 0.83\ lt/min$$

for each hole

3.2 Changing the design of air channels

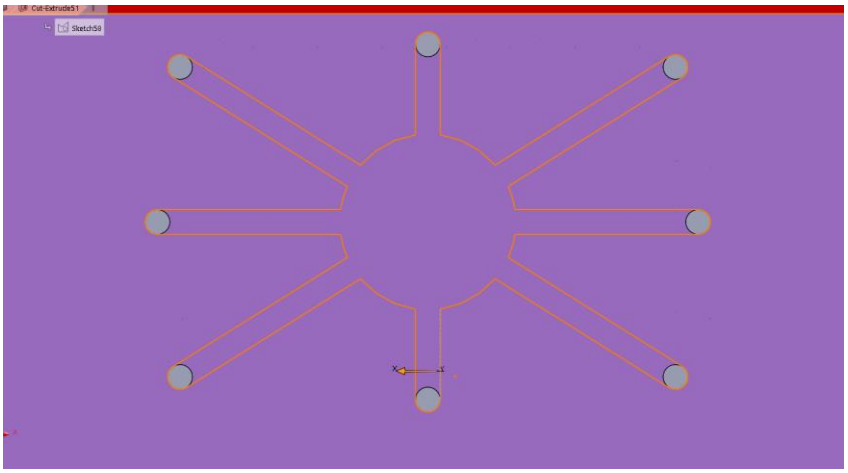

Figure 34: Volume flow rate representation of some holes

In order to reach every hole evenly, we thought any curve or any obstacle must be remove the way that air flows through. The idea behind this is a not complex thing or not need to complex mathematical derivations to obtain, if we compare the shape of air channels on Figure 28 and Figure 33, we can easily see the difference. Since the old air duct design contained much more complex recesses, it is obvious that more labor and time will be lost in the turning and production process of this mold. In addition to that, it has huge negative effect of production cost. Of course there are some rare company applying these analysis to their machines and they gain back so much energy, time, money and high product qualities. We apply this shape to all of our body's face and then investigate again the air distribution through these channels.

3.3 Results of air flow analysis

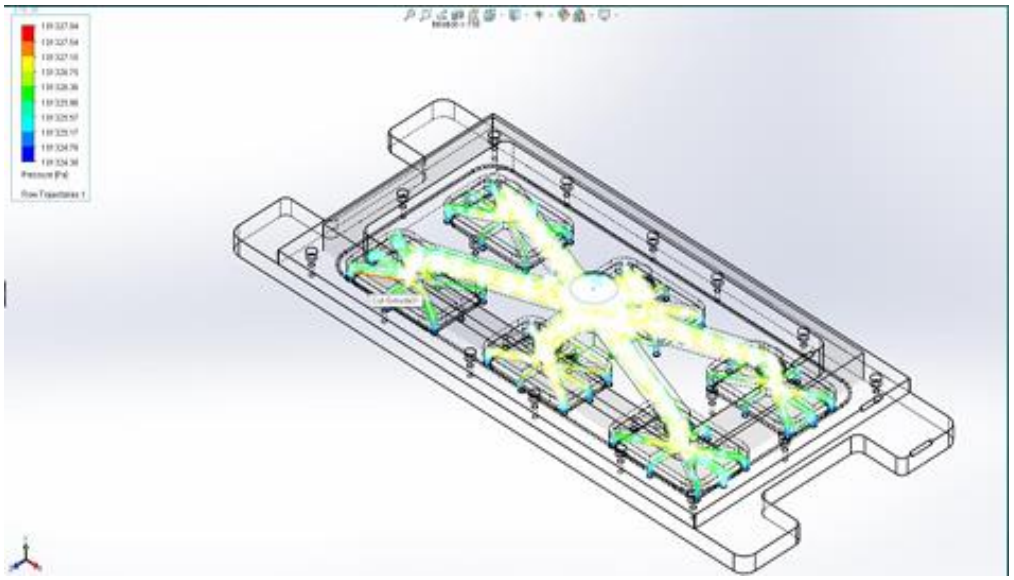

Figure 35: Air pressure and volume flow distribution for new design

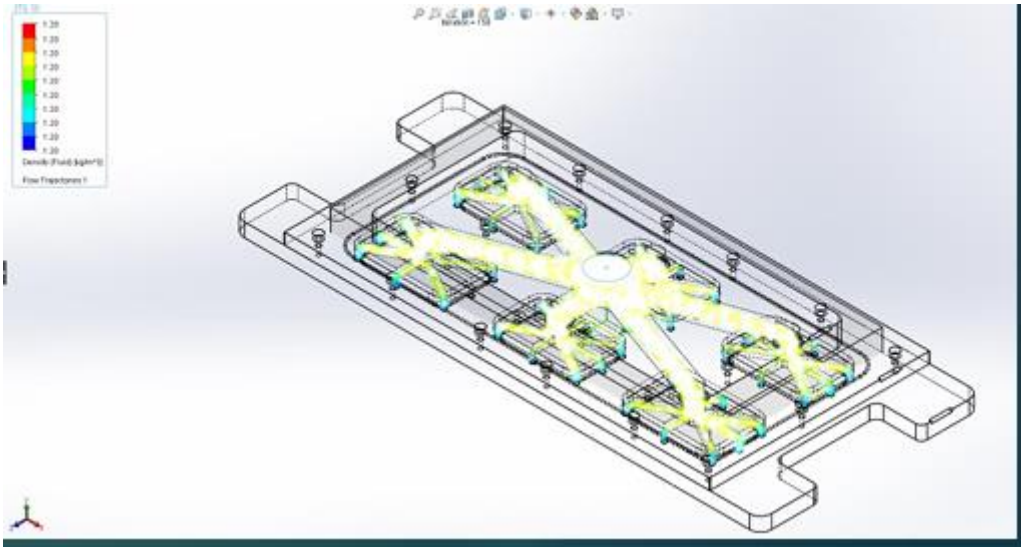

Figure 36: Air pressure and volume flow distribution for new design

As we can see in Figure 35 and Figure 36, the changes we made may be seen simple but the difference is extremely remarkable. As i mentioned before, in our country Turkey, in our thermoform molding market, almost no company have and apply these simple analysis and results. But first let us see the analytical solutions.

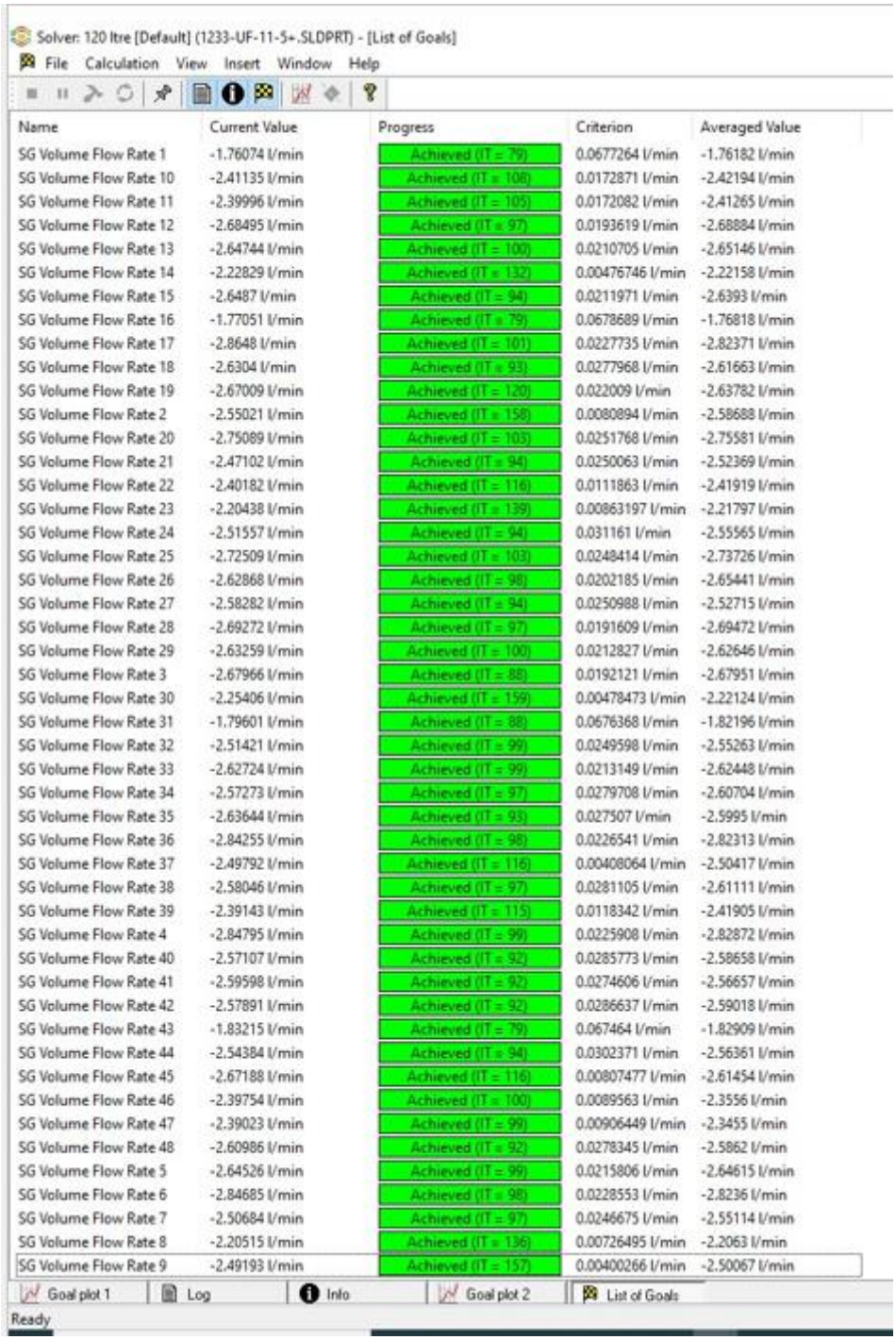

Name	Current Value	Progress	Criterion	Averaged Value
SG Volume Flow Rate 1	-1.76074 l/min	Achieved (IT = 79)	0.0677264 l/min	-1.76182 l/min
SG Volume Flow Rate 10	-2.41135 l/min	Achieved (IT = 108)	0.0172871 l/min	-2.42194 l/min
SG Volume Flow Rate 11	-2.39996 l/min	Achieved (IT = 105)	0.0172082 l/min	-2.41265 l/min
SG Volume Flow Rate 12	-2.68495 l/min	Achieved (IT = 97)	0.0193619 l/min	-2.68884 l/min
SG Volume Flow Rate 13	-2.64744 l/min	Achieved (IT = 100)	0.0210705 l/min	-2.65146 l/min
SG Volume Flow Rate 14	-2.22829 l/min	Achieved (IT = 132)	0.00476746 l/min	-2.22158 l/min
SG Volume Flow Rate 15	-2.6487 l/min	Achieved (IT = 94)	0.0211971 l/min	-2.6393 l/min
SG Volume Flow Rate 16	-1.77051 l/min	Achieved (IT = 79)	0.0678689 l/min	-1.76818 l/min
SG Volume Flow Rate 17	-2.8648 l/min	Achieved (IT = 101)	0.0227735 l/min	-2.82371 l/min
SG Volume Flow Rate 18	-2.6304 l/min	Achieved (IT = 93)	0.0277968 l/min	-2.61663 l/min
SG Volume Flow Rate 19	-2.67009 l/min	Achieved (IT = 120)	0.022009 l/min	-2.63782 l/min
SG Volume Flow Rate 2	-2.55021 l/min	Achieved (IT = 158)	0.0080894 l/min	-2.58688 l/min
SG Volume Flow Rate 20	-2.75089 l/min	Achieved (IT = 103)	0.0251768 l/min	-2.75581 l/min
SG Volume Flow Rate 21	-2.47102 l/min	Achieved (IT = 94)	0.0250063 l/min	-2.52369 l/min
SG Volume Flow Rate 22	-2.40182 l/min	Achieved (IT = 116)	0.0111863 l/min	-2.41919 l/min
SG Volume Flow Rate 23	-2.20438 l/min	Achieved (IT = 139)	0.00863197 l/min	-2.21797 l/min
SG Volume Flow Rate 24	-2.51557 l/min	Achieved (IT = 94)	0.031161 l/min	-2.55565 l/min
SG Volume Flow Rate 25	-2.72509 l/min	Achieved (IT = 103)	0.0248414 l/min	-2.73726 l/min
SG Volume Flow Rate 26	-2.62868 l/min	Achieved (IT = 98)	0.0202185 l/min	-2.65441 l/min
SG Volume Flow Rate 27	-2.58282 l/min	Achieved (IT = 94)	0.0250988 l/min	-2.52715 l/min
SG Volume Flow Rate 28	-2.69272 l/min	Achieved (IT = 97)	0.0191609 l/min	-2.69472 l/min
SG Volume Flow Rate 29	-2.63259 l/min	Achieved (IT = 100)	0.0212827 l/min	-2.62646 l/min
SG Volume Flow Rate 3	-2.67966 l/min	Achieved (IT = 88)	0.0192121 l/min	-2.67951 l/min
SG Volume Flow Rate 30	-2.25406 l/min	Achieved (IT = 159)	0.00478473 l/min	-2.22124 l/min
SG Volume Flow Rate 31	-1.79601 l/min	Achieved (IT = 88)	0.0676368 l/min	-1.82196 l/min
SG Volume Flow Rate 32	-2.51421 l/min	Achieved (IT = 99)	0.0249598 l/min	-2.55263 l/min
SG Volume Flow Rate 33	-2.62724 l/min	Achieved (IT = 99)	0.0213149 l/min	-2.62448 l/min
SG Volume Flow Rate 34	-2.57273 l/min	Achieved (IT = 97)	0.0279708 l/min	-2.60704 l/min
SG Volume Flow Rate 35	-2.63644 l/min	Achieved (IT = 93)	0.027507 l/min	-2.5995 l/min
SG Volume Flow Rate 36	-2.84255 l/min	Achieved (IT = 98)	0.0226541 l/min	-2.82313 l/min
SG Volume Flow Rate 37	-2.49792 l/min	Achieved (IT = 116)	0.00408064 l/min	-2.50417 l/min
SG Volume Flow Rate 38	-2.58046 l/min	Achieved (IT = 97)	0.0281105 l/min	-2.61111 l/min
SG Volume Flow Rate 39	-2.39143 l/min	Achieved (IT = 115)	0.0118342 l/min	-2.41905 l/min
SG Volume Flow Rate 4	-2.84795 l/min	Achieved (IT = 99)	0.0225908 l/min	-2.82872 l/min
SG Volume Flow Rate 40	-2.57107 l/min	Achieved (IT = 92)	0.0285773 l/min	-2.58658 l/min
SG Volume Flow Rate 41	-2.59598 l/min	Achieved (IT = 92)	0.0274606 l/min	-2.56657 l/min
SG Volume Flow Rate 42	-2.57891 l/min	Achieved (IT = 92)	0.0286637 l/min	-2.59018 l/min
SG Volume Flow Rate 43	-1.83215 l/min	Achieved (IT = 79)	0.067464 l/min	-1.82909 l/min
SG Volume Flow Rate 44	-2.54384 l/min	Achieved (IT = 94)	0.0302371 l/min	-2.56361 l/min
SG Volume Flow Rate 45	-2.67188 l/min	Achieved (IT = 116)	0.00807477 l/min	-2.61454 l/min
SG Volume Flow Rate 46	-2.39754 l/min	Achieved (IT = 100)	0.0089563 l/min	-2.3556 l/min
SG Volume Flow Rate 47	-2.39023 l/min	Achieved (IT = 99)	0.00906449 l/min	-2.3455 l/min
SG Volume Flow Rate 48	-2.60986 l/min	Achieved (IT = 92)	0.0278345 l/min	-2.5862 l/min
SG Volume Flow Rate 5	-2.64526 l/min	Achieved (IT = 99)	0.0215806 l/min	-2.64615 l/min
SG Volume Flow Rate 6	-2.84685 l/min	Achieved (IT = 98)	0.0228553 l/min	-2.8236 l/min
SG Volume Flow Rate 7	-2.50684 l/min	Achieved (IT = 97)	0.0246675 l/min	-2.55114 l/min
SG Volume Flow Rate 8	-2.20515 l/min	Achieved (IT = 136)	0.00726495 l/min	-2.2063 l/min
SG Volume Flow Rate 9	-2.49193 l/min	Achieved (IT = 157)	0.00400266 l/min	-2.50067 l/min

Figure 37: Output value of volume flow rate of each hole for new design

We can easily see the effect of how the results change when the shape and number of holes changed.

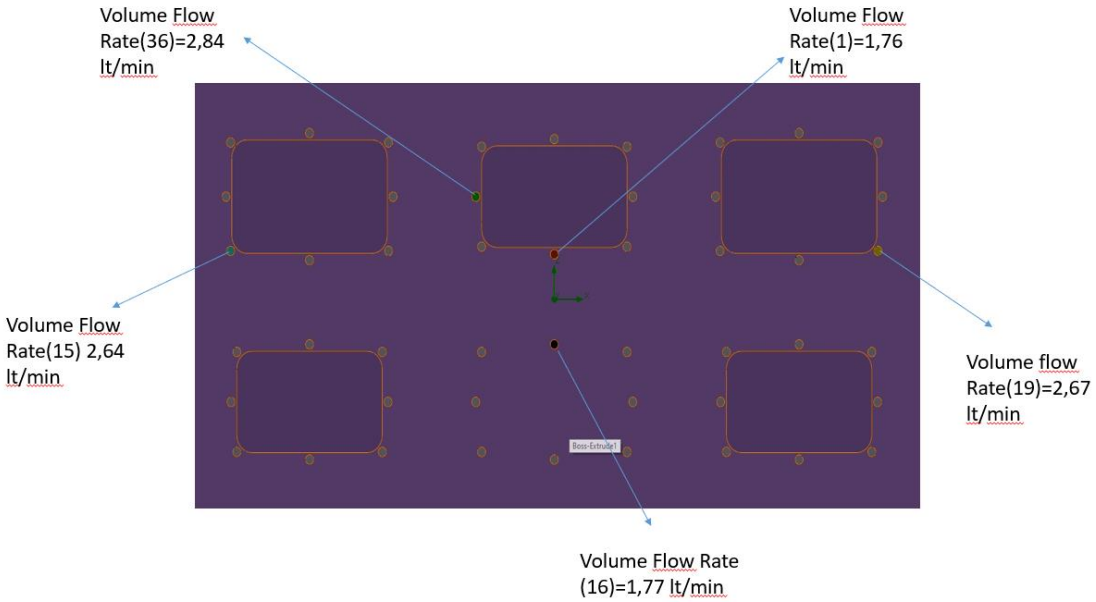

Figure 38: Volume flow rate representation of some holes for new design

At this point, the results show us that changing the shape of air channel and decreasing the number of holes make a huge difference for almost all holes. We obtain the results of volume flow rate value closer to each other for every holes on the part.

Table 6: Results of volume flow rate of some holes of standard design

Volume Flow Rate (36)	**2.842**	**2,36 %**
Volume Flow Rate (1)	1.76	1,47 %
Volume Flow Rate (16)	1.77	1,47 %
Volume Flow Rate (15)	2.64	2,2 %
Volume Flow Rate (19)	2.67	2,225 %

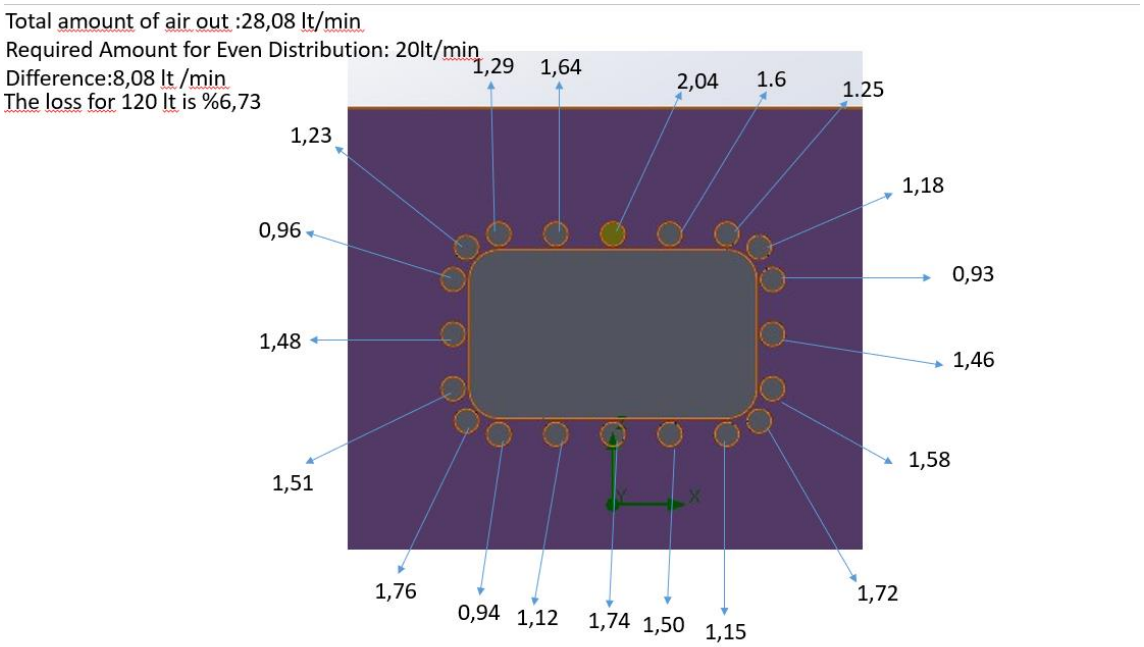

Figure 39: Results that air flow output for a part of old design

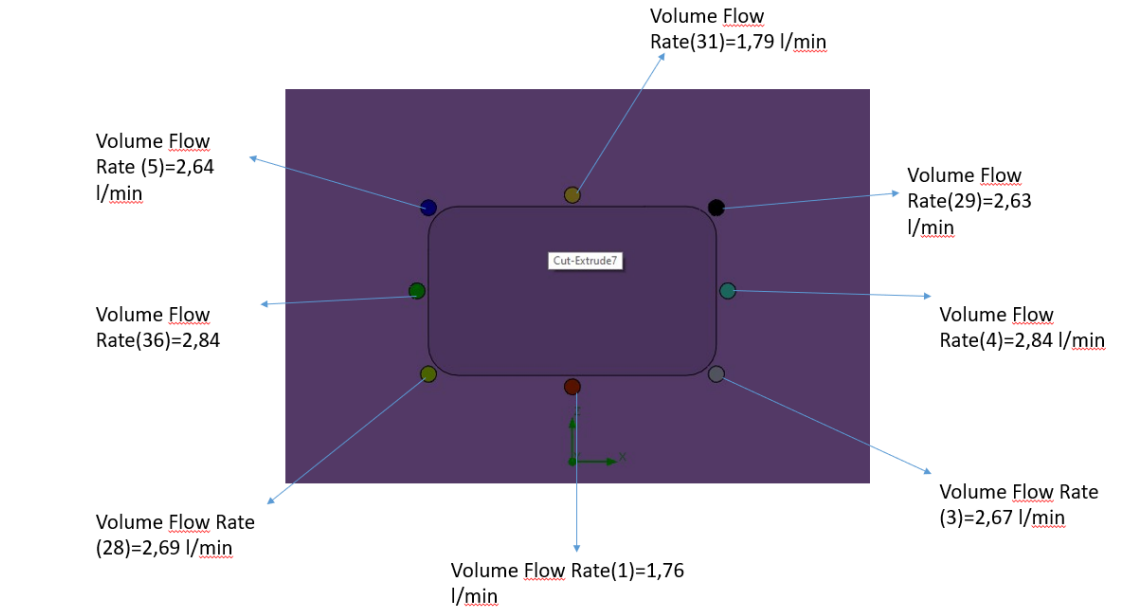

Figure 40: Results that air flow output for a part of new design

3.4 Comparison of the results

We have 48 holes of this part. It can be easily calculate the amount of air coming out of each hole;

$$\frac{120\ lt/min}{48} = 2.5\ lt/min$$

for each hole.

If we compare the results with each other and intend to calculate the loss, there are 6 part that holes around on it for our specimen.

Calculation for old design;

Total amount of air coming out :28,08 lt/min

Required Amount for Even Distribution: 20lt/min

Difference:8,08 lt /min

The loss for 120 lt/min is 6,73 %

Calculation for new design;

Total amount of air coming out: 19.86 lt/min

Required Amount for Even Distribution :20lt /min

Difference:0.14 lt/min

The loss for 120 lt/min is 0,11 %

Table 7: Comparison of new and old design analyzes results

	Results of old design	**Results of new design**
Total amount of air coming out	28,08 lt/min	19.86 lt/min
Required Amount for Even Distribution	20 lt/min	20 lt/min
Difference	8,08 lt/min	0,14 lt/min
Total loss percantage	6,73 %	0,11 %

Results of analyzes show that our new design has remarkable optimization according to these values. Even if there are other plenty of problem that decreases the production efficiency on thermoform molding, our computations and analyzes make these manufacturing processes more efficient. Thus, these improvement can be applied to this industries.

3.5 Cost analysis

An organization's project management and profit forecasting can both benefit from cost analysis. Cost analysis is a tool used by financial experts to determine the potential revenue generated by a project in relation to its total expenditures. Understanding cost analysis and how to calculate it could be beneficial for those working in finance or project management. In this work, The price analysis can be divided into 2 parts. The first is the cost of total of the upper forming materials, and the second is the cost of the lower forming materials. At first we analyze the upper forming parts of the machine.

In these area, aluminium is the best and most common material because of its chemical and phsical properties. The properties of aluminium are;

•**Thermal Conductivity:** Aluminum has high thermal conductivity, allowing the mold surface to reach the desired temperature of the plastic material more quickly during the

thermoforming process. Rapid heat transfer facilitates faster and more homogeneous shaping of the plastic material.

• **Lightweight:** Aluminum is lighter than other metals, enabling easier transportation, processing, and storage of molds. Additionally, its lightweight nature reduces the loads during the production process and promotes energy savings.

• **Durability:** Aluminum is resistant to oxidation and corrosion, ensuring the longevity of molds and maintaining their durability even after repeated use.

• **Machinability:** Aluminum is easy to machine, allowing for shaping through processes like turning, milling, and drilling. This feature enables the easy incorporation of complex shapes and details into molds, providing significant flexibility in design and production.

• **Surface Quality:** Aluminum's naturally smooth surface enhances the surface quality of thermoform molds, enabling precise transfer of desired shapes onto the plastic material and resulting in smoother and more aesthetically pleasing final products.

Table 8: Properties of aluminium

State of matter	**Solid**
Density	2,70 g/cm^3
Density in liquid form	2,375 g/cm^3
Melting point	660,32 °C
Boiling point	2519 °C
Heat of melting	10,71 kJ/mol
Heat of evaporation	294,0 kJ/mol
Heat capacity	24,2 $\frac{J}{mol}.K$

Table 9: Cost analysis of the lower forming parts

Part Name	Material	Count	Weight (kg)	Unit Price (₺)	Material Cost (₺)	Process Cost (₺)	Total Cost (₺)
LF-8-5	5052-H32	1	70.03	135,45	9486	10800	20286
Insert	5052-H32	3	8.736	135,45	1183	14400	15583
Inpart2-1	5052-H32	1	1	135,45	135,45	1200	1335,45
Inpart-1	5052-H32	1	1.4	135,45	190	3600	3790
Inpart -2	5052-H32	1	0.77	135,45	104	3600	3704
LF 4-1-5	5052-H32	1	1	135,45	135,45	1200	1335,45
LF 7-7	7075-T6	1	3.4	196,73	670	4800	5470
LF-11-5	5052-H32	1	9.8	135,45	1327	1200	2527
LF-5-2-5	5052-H32	1	2	135,45	270,90	1200	1470,90
LF-3-2-6	5052-H32	1	1.6	135,45	217	3600	3817
LF-4-2-5	5052-H32	1	1.6	135,45	217	1200	1417
LF-2-2-6	5052-H32	1	0.75	135,45	102	2400	2502
LF-2-3-6	5052-H32	1	0.78	135,45	105	2400	2505
						Total	65742.80

Total cost can be found adding material cost and process cost. The material costs and process costs that we took are the current prices for our country. It can be different from company to company but these values come from the current market prices.

Table 10: Cost analysis of the upper forming parts

Part Name	Material	Count	Weight (kg)	Unit Price (₺)	Material Cost (₺)	Process Cost (₺)	Total Cost (₺)
Plug assist for cup	5052-H32	1	5.80	135,45	785.6	4800	5586
Plug assist for lid	5052-H32	1	6.40	135,45	867	4800	5667
Top plug assist	6061-T6	1	7.1	164,48	1168	4800	5968
UF-11-5-1 (old)	5052-H32	1	31.467	135,45	4262	3600	7862
UF-11-5-2	5052-H32	1	29.368	135,45	3978	3600	7578
UF-11-5-3	5052-H32	1	28.846	135,45	3907	3600	7507
UF-8-5-1	7075-T6	1	12	196,73	2361	3000	5361
UF-8-5-2	5052-H32	1	12.5	135,45	1693	3600	5293
UF-8-5-3	5052-H32	2	7.780	135,45	2108	2400	4508
						Total	49744

As you can see in Table 9 and Table 10, the total costs are 65742.80 ₺ for lower parts, 49744 ₺ for upper parts, if we add up these values;

$$65742.80 + 49744 = 115486.8\,₺$$

is the total production cost for a forming station. This refers to the materials required to produce the mold of a lid and cup product and the total cost required for the labor of these materials.

Table 11: The cost table of old design

Part Name	Material	Count	Weight (kg)	Unit Price (₺)	Material Cost (₺)	Process Cost (₺)	Total Cost (₺)
UF-11-5-1 (old)	5052-H32	1	31.467	135,45	4262	3600	7862
UF-11-5-2	5052-H32	1	29.368	135,45	3978	3600	7578
UF-11-5-3	6061-T6	1	28.846	135,45	3907	3600	7507
						Total	22947

Table 12: The cost table of new design

Part Name	Material	Count	Weight (kg)	Unit Price (₺)	Material Cost (₺)	Process Cost (₺)	Total Cost (₺)
UF-11-5-1 (new)	5052-H32	1	33.201	135,45	4497	3600	8097
UF-11-5-2	5052-H32	1	29.368	135,45	3978	3600	7578
UF-11-5-3	6061-T6	1	28.538	135,45	3865	3600	7465
						Total	23140

As can be seen, the cost difference of the mold with the redesigned air ducts compared to the old design is very close to each other, even the difference is 193 TL. Based on this, it has been proven that the improvement we made does not have any extra cost, and that we will even reduce the cost of turning operations by simplifying the complex structure of the air ducts and reducing the number of holes.

4. CONCLUSION

Many industries, such as those dealing with food, medicine, automobiles, and electronics, rely on thermoforming, a kind of polymer processing. Thermoforming is a straightforward manufacturing technique, but it can be fraught with technical challenges due to the unique processing conditions. These drawbacks should be taken into account right from the start when deciding on processing parameters because they noticeably affect the product's thickness profile. As computing power and processing capacity have increased, numerical simulation has started to supplant the traditional methods of improving process conditions via trial and error. Improving production line control through more accurate end-product forecasting is dependent on include these constraints in simulations, which is still a difficult task. Much work has been put into studying each of these flaws separately and developing more accurate models within the last 20 years. Unfortunately, not enough research has been carried out to fully model the thermoforming process while simultaneously considering all of these factors (which is reflective of the real processing conditions). While there is commercial software that can accurately simulate a product's thermoforming, the majority of these programs are opaque and lack flexible functional flowcharts.

We only change the design of air channels and the number of holes but it creates more considerable differences than the common manufecturing process types on this area.

The simulations and analyzes we made prove that there are remarkable consequences according to our air flow analysis' conclusions. If these optimizations are applied in the real industry, many of company can see the difference. Thanks to these optimizations, these companies will benefit from time, labor and production costs compared to before. In addition, they will produce higher quality products in a faster time and consume less energy. This will significantly increase the quantity and quality of the product produced per unit time.

5. REFERENCES

[1] Koziey BL, Ghafur MO, Vlachopoulos J, Mirza FA. Chapter 3 Computer simulation of thermoforming. Compos Mater Ser 1997; 11:75–89.

[2] Throne JL. Understanding Thermoforming. 2nd ed. 1999.

[3] Rosen SR. A History of the growth of the thermoforming industry. Nature 1979; 19: 381-382.

[4] Plastics T, Size M, Summary R. Thermoformed plastics market size, share & trends analysis report by product (Bio-degradable Polymers, PE, PVC, PP), by process, by application, by region, and segment forecasts,2021-2028, 2021.

[5] McCool R, Martin PJ. The role of process parameters in determining wall thickness distribution in plug-assisted thermoforming. Polym Eng Sci 2010; 50:1923–34.

[6] Giménez E, Lagarón JM, Maspoch ML, Cabedo L, Saura JJ. Uniaxial tensile behavior and thermoforming characteristics of high barrier EVOH-based blends of interest in food packaging. Polym Eng Sci 2004; 44:598–608.

[7] Teck Kim Y, Min B, Won Kim K. General characteristics of packaging materials for food system. Elsevier Ltd; 2013.

[8] Knoeppel D, Sun L, Tippet J. High impact polystyrene with high gloss and high impact strength. WO 2013/154592 Al 2013.

[9] Thelen D, Martin J, Allen S, SA S. Thermoformed Polystyrene Products 2017; 002:7.

[10] Paplham W, Victor J. Process for thermoforming acrylic polymer employing foam as a mold and article formed there from. WO 2010/068787 Al 2010.

[11] Bairagi PD, Darekar AB, Gondker SB, Saudagar RB. Pharmaceutical packaging materials: a brief review. Bairagi Al World J Pharm Pharm Sci 2018; 7:482.

[12] Chawla BPS. Pharmaceutical packaging 1994.

[13] Schüller C, Panozzo D, Grundhöfer A, Zimmer H, Sorkine E, Sorkine-Hornung O. Computational thermoforming. ACM Trans Graph 2016; 35:1–9.

[14] Sharif MFM, Saad AA, Abdullah MZ, Ani FC, Ali MYT, Abdullah MK, et al. A study on thermoforming process ofstretchable circuit and its performance in manufacturing of automotive lighting. AIP Conf Proc 2017; 1901:1–5.

[15] Vanfleteren J, Plovie B, Yang Y, De Smet J, Verplancke R, Bossuyt F, et al. Free-form 2.5D thermoplastic circuits using one-time stretchable interconnections. Mater. Res. Soc. Symp. Proc., vol. 1798, 2015, p. 1–6.

[16] ChoiJ, Han C, Cho S, Kim K, Ahn J, Orbe D Del, et al. Customizable, conformal, and stretchable 3D electronics via predistorted pattern generation and thermoforming. Sci Adv 2021; 7.

[17] Wu K, Zhou Q, Zou H, Leng K, Zeng Y, Wu Z. High precision thermoforming 3D-conformable electronics with a phase-changing adhesion interlayer. Micromachines 2019; 10. [18] Arnold DL. Visor and method of manufacture 2013.

[19] Ashter SA. Review of Characteristics of common plastics for thermoforming. Thermoforming of single and multilayer laminates 2014:39–63.

[20] Erner A. Etude experimentale du thermoformage assiste par poincon d'un melange de polystyrènes. Phd Thesis, Ecole des mines de Paris, 2005.

[21] Atmani O, Abbès F, Li Y, Batkam S, Abbès B. Experimental investigation and constitutive modelling of the deformation behaviour of high impact polystyrene for plug-assisted thermoforming. Mech Ind 2020; 21.

[22] Mieghem B Van. An intelligent experimental approach for the optimisation of the process parameters for the thermoforming of plastics and composites. Phd Thesis, KU Leuven, 2015. [23] Ayadi A, Lacrampe MF, Krawczak P. Bubble assisted vacuum thermoforming: considerations to extend the use of in-situ stereo-DIC measurements to stretching of sagged thermoplastic sheets. Int J Mater Form 2019.

[24] Schmidt FM, Le Maoult Y, Monteix S. Modelling of infrared heating of thermoplastic sheet used in thermoforming process. J Mater Process Technol 2003; 143–144:225–31.

[25] Buffel B, Amerijckx M, Hamblok M, Van Mieghem B, Desplentere F, Van Bael A. Experimental and computational analysis of the heating step during thermoforming of thermoplastics. Key Eng Mater 2015; 651–653:1003–8.

[26] Hmida-Maamar S, Schmidt F, Robert L, Velay V, Mercier D. Identification de paramètres de comportement de membranes en polymères durant le procédé de soufflage. Matériaux Tech 2006;378:371–8.

[27] Marathe D, Rokade D, Busher Azad L, Jadhav K, Mahajan S, Ahmad Z, et al. Effect of plug temperature on the strain and thickness distribution of components made by plug assist thermoforming. Int Polym Process 2016; 31:166–78.

[28] Collins P, Harkin-Jones EMA, Martin PJ. The role of tool/sheet contact in plug-assisted thermoforming. Int Polym Process 2002; 17:361–9.

[29] Aus Der Wiesche S. Industrial thermoforming simulation of automotive fuel tanks. Appl Therm Eng 2004; 24:2391–409.

[30] Khan SA, Girard P, Bhuiyan N, Thomson V. Improved mathematical modeling for the sheet reheat phase during thermoforming. Polym Eng Sci 2012; 52:625–36.

[31] Martin PJ, Duncan P. The role of plug design in determining wall thickness distribution in thermoforming. Polym Eng Sci 2007; 47:804–13.

[32] Sala G, Cassago D, Di Landro L. A numerical and experimental approach to optimise sheet stamping technologies: Polymers thermoforming. Mater Des 2002; 23:21–39.

[33] Kommoji S, Banerjee R, Bhatnagar N, Ghosh AK. Studies on the stretching behaviour of medium gauge high impact polystyrene sheets during positive thermoforming. J Plast Film Sheeting 2015; 31:96–112.

[34] Kouba K, Bartos O, Vlachopoulos J. Computer simulation of thermoforming in complex shapes. Polym Eng Sci 1992; 32:699–704.

[35] Adams AM, Buckley CP, Jones DP. Biaxial hot drawing of poly(ethylene terephthalate): Measurements and modelling of strain-stiffening. Polymer 2000; 41:771–86.

[36] Nardi D, Sinke J. Design analysis for thermoforming of thermoplastic composites: prediction and machine learning-based optimization. Compos Part C Open Access 2021; 5:100126.

[37] Morris BA. Thermoforming, Orientation, and Shrink. 2017.

[38] Wei H, Yan S, Goel S, Menary G. Characterization and modelling the mechanical behaviour of poly (l-lactic acid) for the manufacture of bioresorbable vascular scaffolds by stretch blow moulding. Int J Mater Form 2019.

[39] Antonio Sergio Pouzada , William Andrew Design and Manufacturing of Plastics Products: Integrating Conventional Methods and Innovative Technologies

[40] Azdast T, Doniavi A, Rash Ahmadi S, Amiri E. Numerical and experimental analysis of wall thickness variation of a hemispherical PMMA sheet in thermoforming process. Int J Adv Manuf Technol 2013; 64:113–22.

[41] Khan SA. Improved mathematical model for sheet reheat phase in thermoforming process, Phd thesis, Concordia University. 2009.

[42] Ayadi A, Lacrampe MF, Krawczak P. A comprehensive study of bubble inflation in vacuum assisted thermoforming based on whole-field strain measurements. AIP Conf Proc 2018; 1960.

[43] Bachir-cherif K. Optimisation de l'étape de chauffage infrarouge en thermoformage à l'aide de méta-heuristiques, Phd Thesis, Université du Québec. 2019.

[44] Buffel B, Van Mieghem B, Van Bael A, Desplentere F. A combined experimental and modelling approach towards an optimized heating strategy in thermoforming of thermoplastics sheets. Int Polym Process 2017; 32:378–86.

[45] Chy MI, November PO. Estimation and Control of Plastic Temperature in Heating Phase of Thermoforming Process, Phd Thesis, McGill University. 2013.

[46] Cosson B, Schmidt F, Le Maoult Y, Bordival M. Infrared heating stage simulation of semi transparent media (PET) using ray tracing method. Int J Mater Form 2011; 4:1–10.

[47] Ahmad D. Analyse et simulation de la déformation de films polymères de décoration au cours 38 de leur mise en forme, PhD Thesis, Institut national des sciences appliquées de Lyon. 2013.

[48] Van Mieghem B, Desplentere F, Van Bael A, Ivens J. Improvements in thermoforming simulation by use of 3D digital image correlation. Express Polym Lett 2015; 9:119–28.

[49] Zhang H, Che F, Lin T, Zhao W. Thermal modeling, analysis, and design. 2020.

[50] Morales RA, Candal M V., Santana OO, Gordillo A, Salazar R. Effect of the thermoforming process variables on the sheet friction coefficient. Mater Des 2014; 53:1097–103.

[51] Van Mieghem B, Ivens J, Van Bael A. Consistency of strain fields and thickness distributions in thermoforming experiments through stereo DIC. Exp Tech 2016; 40:1409–20.

[52] Nied HF, Taylor CA, Delorenzi HG. Three-dimensional finite element simulation of thermoforming. Polym Eng Sci 1990; 30:1314–22.

[53] deLorenzi HG, Nied HF. Blow molding and thermoforming of plastics: Finite element modeling. Comput Struct 1987; 26:197–206.

[54] Verron E, Marckmann G, Peseux B. Dynamic inflation of non-linear elastic and viscoelastic rubber-like membranes. International Journal for Numerical Methods in Engineering, 2001: 50(5):1233–51.

[55] Verron E, Khayat R, Derdouri A, Peseux B, Verron E, Khayat R, et al. Dynamic inflation of hyperelastic spherical membranes. Journal of Rheology, 1999; 43(5): 1083-1097.

[56] Erchiqui F, Souli M, Ben YR. Nonisothermal finite-element analysis of thermoforming of polyethylene terephthalate sheet: Incomplete effect of the forming stage. Polym Eng Sci 2007; 47:2129–44.

[57] Schmidt LR, Carley JF. Biaxial stretching of heat-softened plastic sheets: Experiments and results. Polym Eng Sci 1975;15:51–62.

[58] Giacomin AJ, Mix AW, Mahmood O. Sag in thermoforming. Polym Eng Sci 2010; 50:2060–8.

[59] Woelfle C, Koppi K, Costeux S, Hogan T, Dooley J, Van Daele R, et al. Difference in thermoforming processability observed for three high impact polystyrenes. Annu Tech Conf - ANTEC, Conf Proc 2007; 2:1118–22.

[60] Bernard CA, Correia JPM, Bahlouli N, Ahzi S. Numerical simulation of plug-assisted thermoforming process: Application to Polystyrene. Key Eng Mater 2013; 554–557:1602–10.

[61] Dong Y, Lin RJT, Bhattacharyya D. Finite element simulation on thermoforming acrylic sheets Using Dynamic Explicit Method 2006; 14:307–28.

[62] Srivastava V, Chester SA, Ames NM, Anand L. A thermo-mechanically-coupled large deformation theory for amorphous polymers in a temperature range which spans their glass transition. Int J Plast 2010; 26:1138–82.

[63] Derdouri A, Erchiqui F, et al. Viscoelastic behavior of polymer membranes under inflation. Proc Int Congr Rheol 13th, Cambridge, United Kingdom, Aug 20-25, 2000; 3:394–6. 39

[64] Laroche D, Erchiqui F. Experimental and theoretical study of the thermoformability of industrial polymers. J Reinf Plast Compos 2000; 19:230–9.

[65] Erchiqui F, Derdouri A. Analyse expérimentale et numérique du comportement de membranes thermoplastiques en ABS et en HIPS dans le procédé de thermoformage. Can J Chem Eng 2008; 83:527–36. [66] Rachik M, Roelandt JM, Batoz JL. Simulation numérique du soufflage et du thermoformage des plastiques. Rev Eur Des Elem 1994; 3:187–210.

[67] Dong Y, Lin RJT, Bhattacharyya D. Determination of critical material parameters for numerical simulation of acrylic sheet forming. J Mater Sci 2005; 40:399–410.

[68] Nam GJ, Ahn KH, Lee JW. Three-dimensional simulation of thermoforming process and its comparison with experiments. Polym Eng Sci 2000; 40:2232–40.

[69] Lee JK, Virkler TL, Scott CE. Effects of rheological properties and processing parameters on ABS thermoforming. Polym Eng Sci 2001; 41:240–61.

[70] Novotný P, Sáha P, Kouba K. Fitting of K-BKZ model parameters for the simulation of thermoforming. Int Polym Process 1999; 14:291–5.

[71] Song WN, Mirza FA, Vlachopoulos J. Finite element analysis of inflation of an axisymmetric sheet of finite thickness. J Rheol 2002; 35:93–111.

[72] Ordonez AS. Damage and modelling of composite materials for the automotive industry, Phd Thesis, Polytech University of Catalunya. 2017.

[73] Suchocki C. Finite element implementation of slightly compressible and incompressible first invariant-based hyperelasticity. J Th Ap Mech 2017; 55:787.

[74] Zamani NG, Watt DF, Esteghamatian M. Status of the finite element method in the thermoforming process. Int J Numer Methods Eng 1989; 28:2681–93.

[75] Carlone P, Palazzo GS. Finite element analysis of the thermoforming manufacturing process using the hyperelastic Mooney-Rivlin model. Lect Notes Comput Sci (Including Subser Lect Notes Artif Intell Lect Notes Bioinformatics) 2006; 3980 LNCS:794–803.

[76] Brennen CE. Constitutive laws. An Internet B Fluid Dyn 2016; 910:63–103.

[77] Oueslati Z. Modèle de comportement pour la modélisation du thermoformage de feuilles plastiques multicouches, PhD Thesis, Université de Technologie de Compiègne. 2015.

[78] Batra R. Elements of Continuum Mechanics. vol. 33. 1988.

[79] Maurel-Pantel A, Baquet E, Bikard J, Bouvard JL, Billon N. A thermo-mechanical large deformation constitutive model for polymers based on material network description: Application to a semi-crystalline polyamide 66. Int J Plast 2015; 67:102–26.

[80] Marckmann G, Verron E. Comparison of hyperelastic models for rubber-like materials. Rubber Chem Technol Am Chem Soc 2006; 79:835–58. 40

[81] Oueslati Z, Rachik M, Lacrampe MF. Transversely isotropic hyperelastic constitutive models for plastic thermoforming simulation. Key Eng Mater 2013; 554–557:1715–28.

[82] Atmani O, Abbès B, Abbès F, Li YM, Batkam S. Identification of a thermo-elasto-viscoplastic behavior law for the simulation of thermoforming of high impact polystyrene. AIP Conf Proc 2018; 1960:1–7.

[83] Erchiqui F. Thermodynamic approach of inflation process of K-BKZ polymer sheet with respect to thermoforming. Polym Eng Sci 2005; 45:1319–35.

[84] Sukiman MS, Erchiqui F, Kanit T, Imad A. Design and numerical modeling of the thermoforming process of a WPC based formwork structure. Mater Today Commun 2020; 22:100805.

[85] Hayden K Webb, Jaimys Arnott, Russel Crawford, Elena P. Ivanova Plastic Degradation and Its Environmental Implications with Special Reference to Poly(ethylene terephthalate)